A GENERAL APPROACH TO COMMON-MODE SIGNAL REJECTION WITH APPLICATION TO MYO-ELECTRIC SIGNAL MEASUREMENTS

by

© H.R. HAYES, B.Sc.

A Thesis

Submitted to the School of Graduate Studies

in Partial Fulfilment of the Requirements

for the Degree

Master of Engineering

McMaster University

April 1979

A GENERAL APPROACH TO COMMON-MODE SIGNAL REJECTION

MASTER OF ENGINEERING (1979)
(Electrical Engineering)

McMASTER UNIVERSITY
Hamilton, Ontario

TITLE: A General Approach to Common-Mode Signal Rejection with Application to Myo-electric Signal Measurements

AUTHOR: Hasler Rudy Hayes, B.Sc. (Sir George Williams University)

SUPERVISORS: Assoc. Professor H.D. Barber

Assoc. Professor S.H. Chisholm

NUMBER OF PAGES: xiii, 87

ABSTRACT

A typical instrumentation problem is the detection of a differential signal in the presence of a common-mode signal. In the case of measuring myo-electric signals, the common-mode signals present can be 10^2-10^4 larger than the differential signal. In such instances, the attenuation of these unwanted common-mode signals require complex circuit designs.

In this work an investigation of the common-mode signal path led to the development of a general approach to the problem of unwanted signals arising from common-mode signal sources. It was found possible to write the overall common-mode gain as a product of the differential amplifier common-mode response and the isolation gain. The isolation gain depends on the ratio of the impedance of the common-mode signal path to the differential amplifier input impedance. The impedance of the common-mode signal path may be increased by employing in the amplifier system a self-contained power supply and an output coupler device such as a transformer.

The general approach was used to design an amplifier system to measure myo-electric signals. This amplifier system gave a much improved common-mode signal rejection

over currently used systems which typically have 40 db of differential gain but only -30 db of common-mode gain at 60Hz. The improvement in common-mode signal rejection was 25 db.

ACKNOWLEDGEMENTS

I wish to extend my deepest appreciation to my supervisors, Dr. D.H. Barber, Ph.D., M.Sc., P.Eng., and Dr. S.H. Chisholm, Ph.D., B.A.Sc., for their encouragement and support.

TABLE OF CONTENTS

TABLE OF CONTENTS (continued)

TABLE OF CONTENTS (continued)

LIST OF ILLUSTRATIONS

LIST OF ILLUSTRATIONS (continued)

LIST OF ILLUSTRATIONS (continued)

LIST OF ILLUSTRATIONS (continued)

LIST OF TABLES

CHAPTER 1

INTRODUCTION

1.1 Introduction

Frequently it is necessary to detect and amplify a small difference signal between two points in the presence of a larger signal common to both points. This signal common to both points is referred to as a common-mode signal. In such situations, an amplifier system is designed which exhibits a high amplification of the differential signal and a much lower amplification of the common-mode signal. There are two approaches that are typically used to minimize the effects of unwanted common-mode signals.

One approach is to use a bandpass amplifier, but this is only possible if the frequency spectrums of the common-mode signal and the differential signal are sufficiently separated so that the common-mode signal frequency is not in the passband.

Another approach employs the symmetry of a differential amplifier as shown in Fig. 1.1(a) to make the amplifier insensitive to common-mode signals. Many circuit designs [1,2] have been made in attempts to approximate more closely the ideal differential amplifier and thus

Fig. 1.1 Methods to reduce the effects of unwanted common-mode signals

(a) Differential amplifier

(b) The common-mode signal paths through (a)

(c) The differential amplifier with a self-contained power supply and an ideal output coupler device

(d) A generalized model of (c) with a non-ideal output coupler device

a)

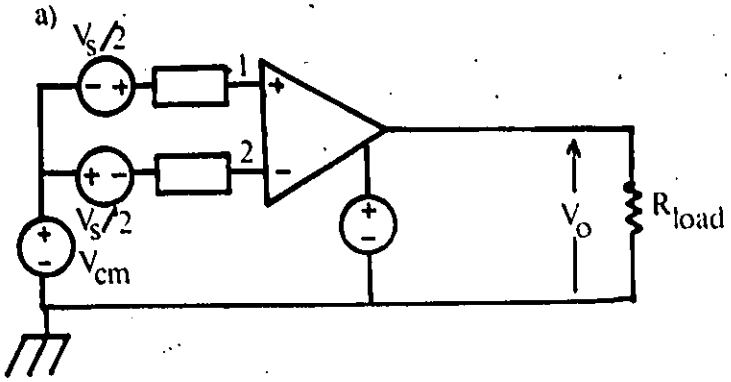
$V_s/2$
1
2
$V_s/2$
V_{cm}
V_o
R_{load}

b)

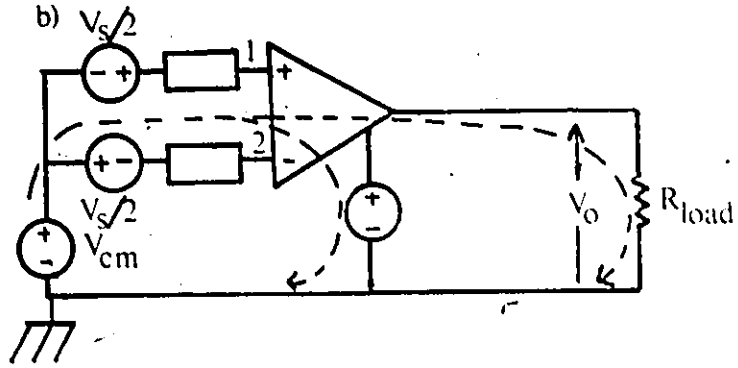
$V_s/2$
1
2
$V_s/2$
V_{cm}
V_o
R_{load}

c)

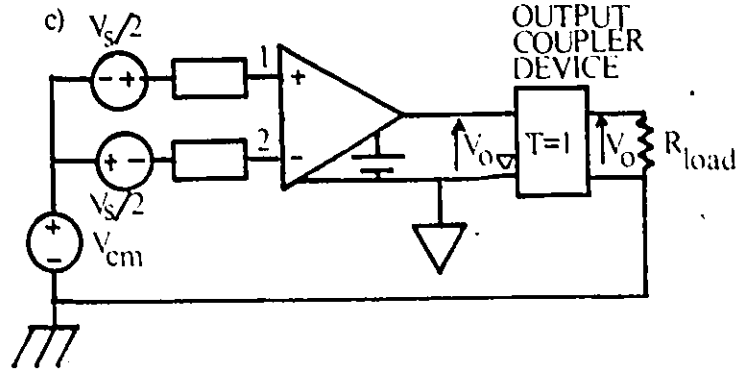
$V_s/2$
OUTPUT
COUPLER
DEVICE
1
2
V_o
T=1
V_o
R_{load}
$V_s/2$
V_{cm}

d)

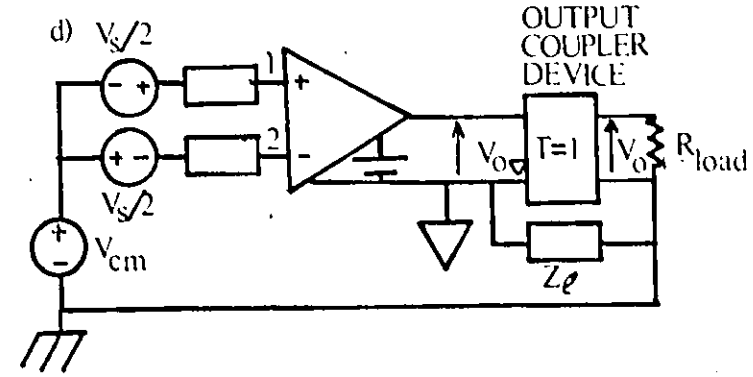
$V_s/2$
OUTPUT
COUPLER
DEVICE
1
2
V_o
T=1
V_o
R_{load}
$V_s/2$
V_{cm}
Z_ℓ

achieve low sensitivity to common-mode signals.

There are some disadvantages to the above approaches. Bulkiness due to circuit complexity and the resulting inability to mount the amplifier sufficiently close to the electrodes to avoid motion artifacts, is an example of one of the drawbacks that can arise.

In this work the common-mode signal path was investigated in order to determine if other methods of reducing the effects of common-mode signals could be realized. This led to a more general approach to the problem of reducing the effects of common-mode signals.

An amplifier system to detect and amplify myoelectric signals was designed utilizing this general approach, which has demonstrated experimentally that the expected improvement in common-mode signal rejection was in fact realized.

1.2 The Concept

Two common-mode signal paths exist in Fig. 1.1(a), as clearly indicated in Fig. 1.1(b), one through the output stage of the amplifier and the other through the power supply. If the common-mode signal paths could be broken, the problem of unwanted effects arising from common-mode sources would not exist.

The common-mode signal path through the power supply

may be easily broken if the power supply of the amplifier can be disconnected from system ground. The use of a battery as a self-contained power supply is one solution. To break the common-mode signal path through the amplifier system, an output coupler device must be used which has the following properties:

1) a four terminal device with its output a function of its differential input,
2) the impedance between its input and output terminal pairs, called the isolation impedance, should be infinite.

If such an ideal output coupler device could be found, the only output signal from such an amplifier system would be due to a differential input signal as no signal path would exist for the common-mode signal as shown in Fig. 1.1(c).

Unfortunately, practical output coupler devices such as transformers, optical couplers and communication links are all characterized by a finite isolation impedance which is hereafter denoted by Z_i. This imperfection means that the common-mode signal path is not completely broken and thus common-mode signal rejection remains a problem. A general approach to the problem of unwanted output signals arising from common-mode signal sources can be developed which includes the non-ideal properties of both the differential amplifier and the output coupler device as

shown in Fig. 1.1(d), which represents a more generalized system model.

1.3 Terminology and Symbology

Two distinct voltage reference nodes or grounds, are used: system ground which is denoted by the symbol ⏚, and local ground which is the differential amplifier internal reference node and is denoted by the symbol ▽. Any variable or network function with the subscript v, is referenced to local ground, while if no such subscript is used, system ground is implied.

The term "differential amplifier" refers to only that portion of the amplifier characterized by a differential gain A_d and a common-mode gain A_{cv}.

$$V_{0v} = A_d (V_1 - V_2) + A_{cv} \frac{(V_{1v} + V_{2v})}{2} \tag{1.1}$$

The output coupler device is characterized by a transfer function T, which includes the transfer function of any associated circuitry.

$$V_0 = T V_{0v} \tag{1.2}$$

For convenience, T will be assumed to be unity unless otherwise stated.

The term "amplifier system", refers to the differential amplifier and the output coupler device.

A_I will be used to designate the isolation gain which is the ratio of the common-mode input signal level with respect to local ground, to the common-mode input signal level with respect to system ground.

$$A_I = \frac{(V_{1v} + V_{2v})/2}{(V_1 + V_2)/2} \tag{1.3}$$

Substitution of (1.2) and (1.3) into (1.1) gives

$$V_0 = A_d\ (V_1 - V_2) + A_{cv}\ A_I\ \frac{(V_1 + V_2)}{2} \tag{1.4}$$

and the amplifier system common-mode gain A_c is

$$A_c = A_{cv}\ A_I \tag{1.5}$$

Note that (1.4) is quite general, for the design approaches of Fig. 1.1(a) and Fig. 1.1(c) are just special cases of $A_I = 1$ and $A_I = 0$ respectively. Figure 1.1(d) is then a more general representation of any amplifier system used to reduce the effects of unwanted common-mode signals, with

$$0 \leq |A_I| \leq 1 \tag{1.6}$$

1.4 Outline

Chapter Two presents an analysis of the circuit model representing the more general approach to the reduction of unwanted common-mode signals, with various simplifying assumptions. As a first approximation, the non-ideal

properties of the output coupler device are modelled by an isolation impedance Z_ℓ which is assumed to consist of a resistor and capacitor in parallel. When used to model the isolation properties of a transformer as the output coupler device, the theory and computer simulation results are shown to be in good agreement with experimental data.

The requirements placed on the amplifier system to measure myo-electric signals (EMG) are presented in Chapter Three for gold electrodes of area 2 cm^2, with a fixed center to center spacing of 2.2 cm. It is shown that the magnitude of the common-mode signal depends on whether or not a system ground connection to the patient is used.

In order to implement a differential amplifier, two subcircuit amplifiers are used. These subcircuit amplifiers are characterized in Appendix A as finite-gain single-pole voltage amplifiers. A novel feature concerning these subcircuit amplifiers is that proper dc bias requires only a single 1.5 volt supply. The subcircuit amplifiers are used to implement a differential amplifier, which is a modified version of a known circuit. Chapter Four presents the theory of this differential amplifier in terms of its differential gain A_d, and common-mode gain A_{cv}.

All the information of the previous chapters is utilized in Chapter Five in designing an amplifier system to measure EMG signals. This design is superior to a currently

used system [10], for it has a bandpass response with a midband gain of 40 db, a second-order low-frequency response with -3 db frequency point at 8 Hz, and a first-order high-frequency response with a -3 db frequency point at 1 kHz. Of greater importance is the improvement of the common-mode gain, which is -55 db at 60 Hz versus -30 db for the currently used system. The chapter concludes with electromyograms taken using this amplifier system with a transformer as the output coupler device.

Extensive use is made of an electronic circuit simulator program, SPICE 2 [3], which is used to verify theory and to show in more detail the effect of various circuit parameters effecting the circuit frequency responses.

CHAPTER 2

AN ANALYSIS OF A GENERALIZED AMPLIFIER SYSTEM MODEL

2.1 Introduction

An analysis of a generalized amplifier system model is presented, using as an example a system to measure EMG signals as shown in Fig. 2.1. Results of the analysis showed that the common-mode gain is determined by:

1) the differential amplifier common-mode response, A_{cv},
2) the impedance of the differential signal source, Z_{skin},
3) the isolation impedance, Z_{ℓ},
4) the differential amplifier input impedance, 2 x $(Z_{id}/2)$,
5) the impedance Z_{cc} of the input coupling capacitor C_c.

An assumption is made in both the analysis and the computer simulation that Z_{ℓ} may be modelled as a resistance and capacitance in parallel between local ground and system ground. To check the analysis and to verify the assumptions made, the differential amplifier of Chapter Four is used. With a transformer as the output coupler device,

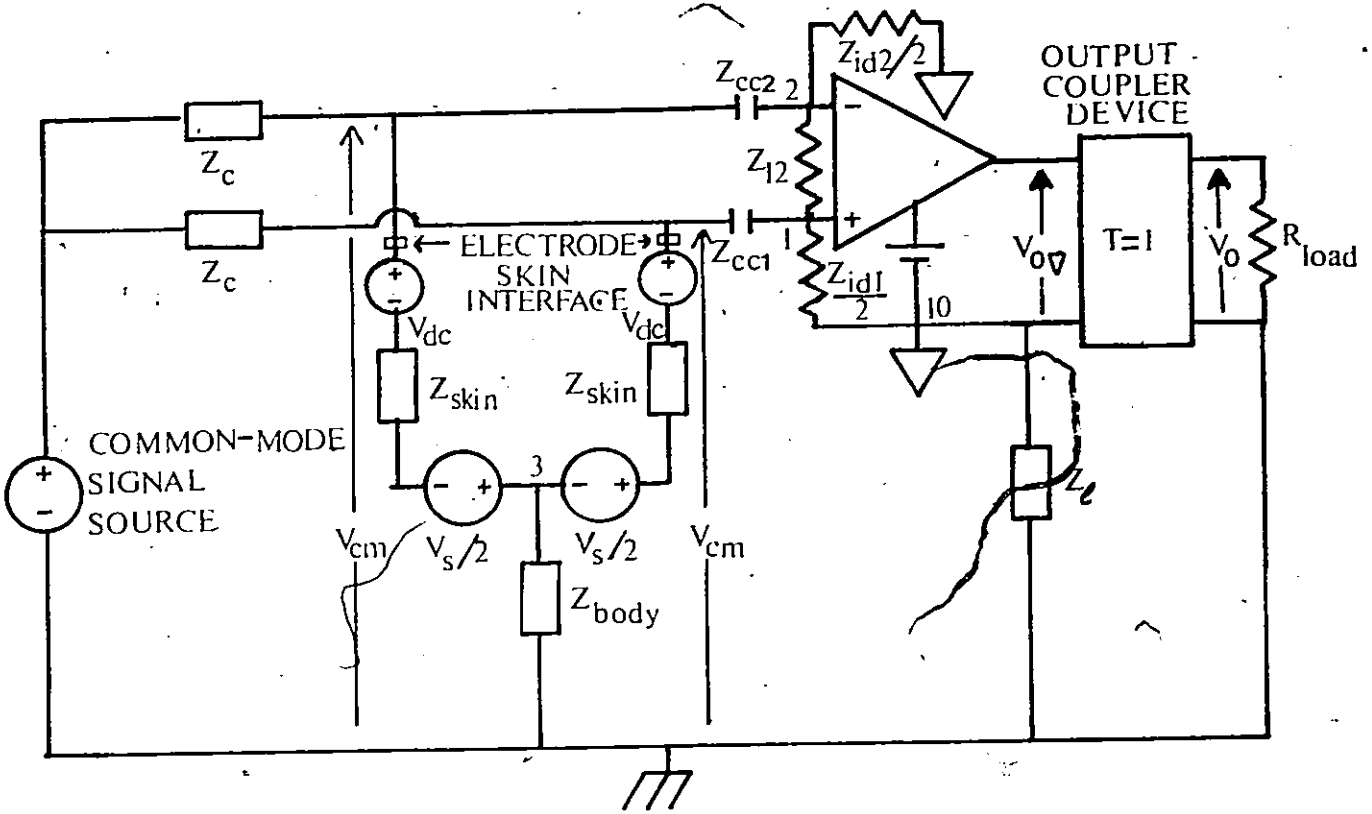

Fig. 2.1 General system model

experimental data, computer simulation and theoretical results from the analysis, exhibit good agreement with one another.

2.2 Analysis of the Generalized Amplifier System

As an initial assumption, perfect symmetry is assumed

$$\Delta Z_{cc} = Z_{cc1} - Z_{cc2} = 0 \tag{2.1}$$

$$\Delta Z_{id} = Z_{id1} - Z_{id2} = 0 \tag{2.2}$$

It is also assumed that differential amplifier input impedance Z'_{id}

$$Z'_{id} = \frac{Z_{id}\, Z_{12}}{Z_{id} + Z_{12}} \simeq Z_{id} \tag{2.3}$$

As a further assumption, the coupling impedance Z_c is

$$Z_c >> Z_{skin} + Z_{body} \tag{2.4}$$

For the differential case, let $V_{cm} = 0$. Then by symmetry at node 3

$$V_{1v} = -V_{2v} = \frac{\frac{V_s}{2} \quad \frac{Z_{id}}{2}}{(Z_{id}/2)+Z_{skin}+Z_{cc}} \tag{2.5}$$

Hence,

$$V_{0d} = A_d\,(V_{1v} - V_{2v}) = \frac{A_d\, V_s\, (Z_{id}/2)}{(Z_{id}/2) + Z_{skin} + Z_{cc}} \tag{2.6}$$

For the common-mode case, let $V_s = 0$. Then

$$V_{1v} = V_{2v} = V_{cm} \frac{(Z_{id}/2)}{(Z_{id}/2) + Z_{cc} + Z_{\ell}} \tag{2.7}$$

Hence,

$$V_{0c} = A_{cv} \frac{(V_{1v} + V_{2v})}{2} = \frac{A_{cv} V_{cm} (Z_{id}/2)}{(Z_{id}/2) + Z_{cc} + Z_{\ell}} \tag{2.8}$$

For the general case, neither the common-mode source nor the differential source are zero, and by superposition

$$V_0 = V_{0d} + V_{0c} \tag{2.9}$$

Substitution into, and rearrangement of, (2.9) yields

$$V_0 = \frac{A_d Z_{id}}{Z_{id}+2Z_{skin}+2Z_{cc}} [V_s + V_{cm} (\frac{A_{cv}}{A_d}) \frac{Z_{id}/2 + Z_{skin} + Z_{cc}}{Z_{id}/2 + Z_{cc} + Z_{\ell}}] \tag{2.10}$$

If the differential input impedance is large with respect to the source impedance,

$$(Z_{id}/2) >> Z_{skin} \tag{2.11}$$

then

$$V_0 = \frac{A_d Z_{id}}{Z_{id}+2Z_{cc}} [V_s + V_{cm} (\frac{A_{cv}}{A_d}) \frac{Z_{id}+2Z_{cc}}{Z_{id}+2Z_{cc}+2Z_{\ell}}] \tag{2.12}$$

By definition, the common-mode rejection ratio is

$$CMRR = \frac{A_c}{A_d} \tag{2.13}$$

Therefore, in this case

$$A_c = \frac{A_{cv}\ (Z_{id})}{(Z_{id} + 2Z_\ell + 2Z_{cc})} \tag{2.14}$$

and

$$CMRR = \frac{A_{cv}}{A_d}\ \frac{(Z_{id})}{(Z_{id} + 2Z_\ell + 2Z_{cc})} \tag{2.15}$$

If

$$Z_\ell = 0\ , \tag{2.16}$$

then (2.15) is the normally found situation, as shown in Fig. 1.1(a), of

$$CMRR = \frac{A_{cv}}{A_d} \tag{2.17}$$

However, if

$$2Z_\ell >> Z_{id} \tag{2.18}$$

a significant improvement in CMRR will result without affecting the gain of the differential signal.

The isolation impedance Z_ℓ of practical output coupler devices such as transformers, optical couplers and transmission links will be modelled to a first approximation as

$$Z_\ell = [G_\ell + sC_\ell]^{-1} \tag{2.19}$$

The isolation gain is then by definition (1.5),

$$A_I = \frac{Z_{id}}{(Z_{id} + 2Z_\ell + 2Z_{cc})} \tag{2.20}$$

Substitution of (2.19) gives

$$A_I = \frac{sC_c \; Z_{id} \; (G_\ell + sC_\ell)}{s^2 C_c C_\ell Z_{id} + s[Z_{id} G_\ell C_c + 2C_c + 2C_\ell] + 2G_\ell} \qquad (2.21)$$

Assuming Z_{id} is constant with frequency

$$Z_{id} = R_{id} \qquad (2.22)$$

Then

$$A_I = \frac{s \; K_I \; (s - z_{I1})}{(s - p_{I1}) \; (s - p_{I2})} \qquad (2.23)$$

with

$$K_I = G_{cc}/G_{id} \qquad (2.24)$$

$$z_{I1} = -G_\ell/C_\ell \qquad (2.25)$$

$$p_{I1} = - \frac{G_\ell \; C_c + 2G_{id} \; C_c + 2G_{id} \; C_\ell}{C_c \; C_\ell} \qquad (2.26)$$

$$p_{I2} = - \frac{2G_\ell \; G_{id}}{G_\ell \; C_c + 2G_{id} \; C_c + 2G_{id} \; C_\ell} \qquad (2.27)$$

If the previous assumption of perfect symmetry is removed, then mismatches in the Z_{cc}'s, Z_{id}'s and Z_{skin}'s can result in the common-mode signal giving rise to a differential signal at the input terminals of the amplifier. This signal is amplified by the differential gain. Inspection of Fig. 2.1, will show that any mismatch of Z_{skin} or Z_c may be considered in terms of a mismatch of Z_{cc}. Therefore to simplify the problem, any mismatch will be represented by

$$\Delta Z_{id} = Z_{id1} - Z_{id2} \qquad (2.28)$$

$$\Delta Z_{cc} = Z_{cc1} - Z_{cc2} \tag{2.29}$$

then the resulting output, V_{omis}, is

$$V_{omis} = \frac{A_d A_I V_{cm}}{2} \left[\frac{Z_{id}\Delta Z_{cc} - 2Z_{cc}\Delta Z_{id} - 2Z_{\ell}\Delta Z_{id}}{(Z_{id} + 2Z_{cc} + 2Z_{\ell})(Z_{id} + 2Z_{cc})}\right] \tag{2.30}$$

By superposition and rearrangement of (2.12),

$$V_0 = \frac{A_d Z_{id}}{Z_{id}+2Z_{cc}} \{V_s + V_{cm} \cdot$$

$$\left[\frac{(Z_{id}\Delta Z_{cc} - 2Z_{cc}\Delta Z_{id} - 2Z_{\ell}\Delta Z_{id})}{2(Z_{id} + 2Z_{cc} + 2Z_{\ell})Z_{id}} A_I + \frac{A_{cv}(Z_{id}+2Z_{cc})}{A_d (Z_{id}+2Z_{cc}+2Z_{\ell})}\right]\} \tag{2.31}$$

For the case as shown in Fig. 1.1(a) where

$$Z_{\ell} = 0 \tag{2.32}$$

and if it is further assumed that

$$Z_{id} >> Z_{cc} \tag{2.33}$$

Then (2.31) is

$$V_0 = \frac{A_d Z_{id}}{Z_{id}+2Z_{cc}} \{V_s + V_{cm} \left[\frac{\Delta Z_{cc}}{2Z_{id}} - \frac{2Z_{cc}\Delta Z_{id}}{2Z_{id}Z_{id}} + \frac{A_{cv}(Z_{id}+2Z_{cc})}{A_d Z_{id}}\right]\} \tag{2.34}$$

The dominating mismatch factor, ΔZ_{cc}, can not be readily trimmed and therefore the common-mode response of the amplifier system will be sensitive to this mismatch. However, if

$$Z_{\ell} \neq 0 \tag{2.35}$$

and if it is assumed that

$$Z_\ell >> Z_{id} \tag{2.36}$$

$$Z_{id} >> Z_{cc} \tag{2.37}$$

then (2.31) becomes

$$V_0 = \frac{A_d Z_{id}}{Z_{id}+2Z_{cc}} \{V_s + V_{cm} \cdot$$

$$[A_I \frac{\Delta Z_{cc}}{4Z_\ell} - A_I \frac{2Z_{cc}\Delta Z_{id}}{4Z_\ell Z_{id}} - A_I \frac{\Delta Z_{id}}{2Z_{id}} + \frac{A_{cv} Z_{id}}{A_d(Z_{id}+2Z_\ell)}]\} \tag{2.38}$$

In comparison to (2.34), the dominating mismatch factor is the differental amplifier input impedance, Z_{id}, which may be easily trimmed by careful selection of components.

It may be seen from the above, that any source mismatch prior to the input terminals of the differential amplifier is divided by the isolation impedance Z_ℓ. Thus in addition to reducing A_c, this same isolation impedance reduces the effects of source mismatch.

As a simplification, ΔZ_{id} and ΔZ_{cc} are assumed hereafter to be zero, unless otherwise stated.

2.3 Verification of the Analysis

The differential amplifier of Chapter Four will be used to verify (2.14) and (2.19). First, good agreement will be shown between theory and computer simulation results using an output coupler device characterized by isolation impedance parameters

$$R_\ell = 10\ G\Omega \tag{2.39}$$

$$C_\ell = 100\ pF \tag{2.40}$$

The differential amplifier common-mode response, A_{cv} is shown in Fig. 2.2 (computer simulation result) and can be characterized by

$$A_{cv} = \begin{cases} A_{cvHo} \dfrac{(s - z_{cH1})}{(s-p_{cH1})(s-p_{cH2})} & \text{at H.F.} \\ A_{cvLo} \dfrac{(s/z_{cL1} - 1)(s/z_{cL2} - 1)}{(s/p_{cL1} - 1)(s/p_{cL2} - 1)} & \text{at L.F.} \end{cases} \tag{4.60}$$

Z_{cc} is the impedance of an input coupler capacitor of value 0.047 μF, and

$$R_{id} = 1\ M\Omega \tag{2.41}$$

Asymptotically plotted theory and computer simulation results for A_c are shown in Fig. 2.3, which shows excellent agreement and indicates that no significant misunderstanding exists by interpreting the computer simulation results in terms of (2.14) and (2.19).

Now, (2.14) and (2.19) will be experimentally verified by showing excellent agreement between computer simulation results and experimental data. The results are obtained with the same differential amplifier as above and a transformer as the output coupler device characterized by isolation impedance parameters

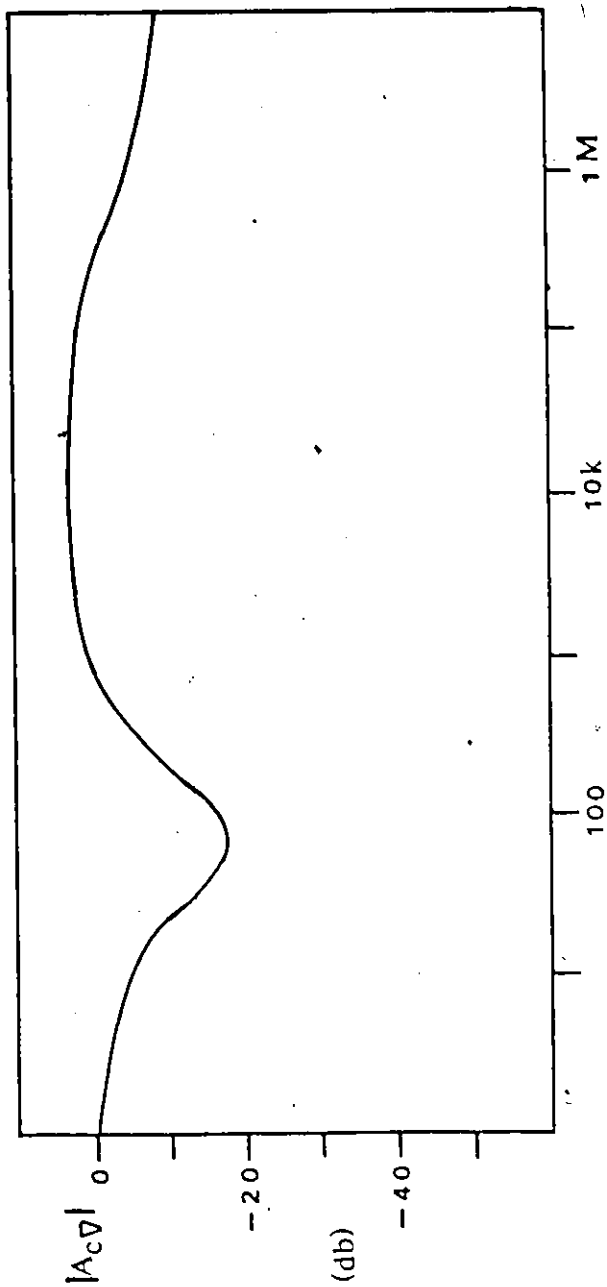

Fig. 2.2 Frequency response of $|A_{CD}|$ for the differential amplifier of Chapter 4, R_{e1}=10kΩ, R_{e2}=1.8kΩ, I_C=2.8μA

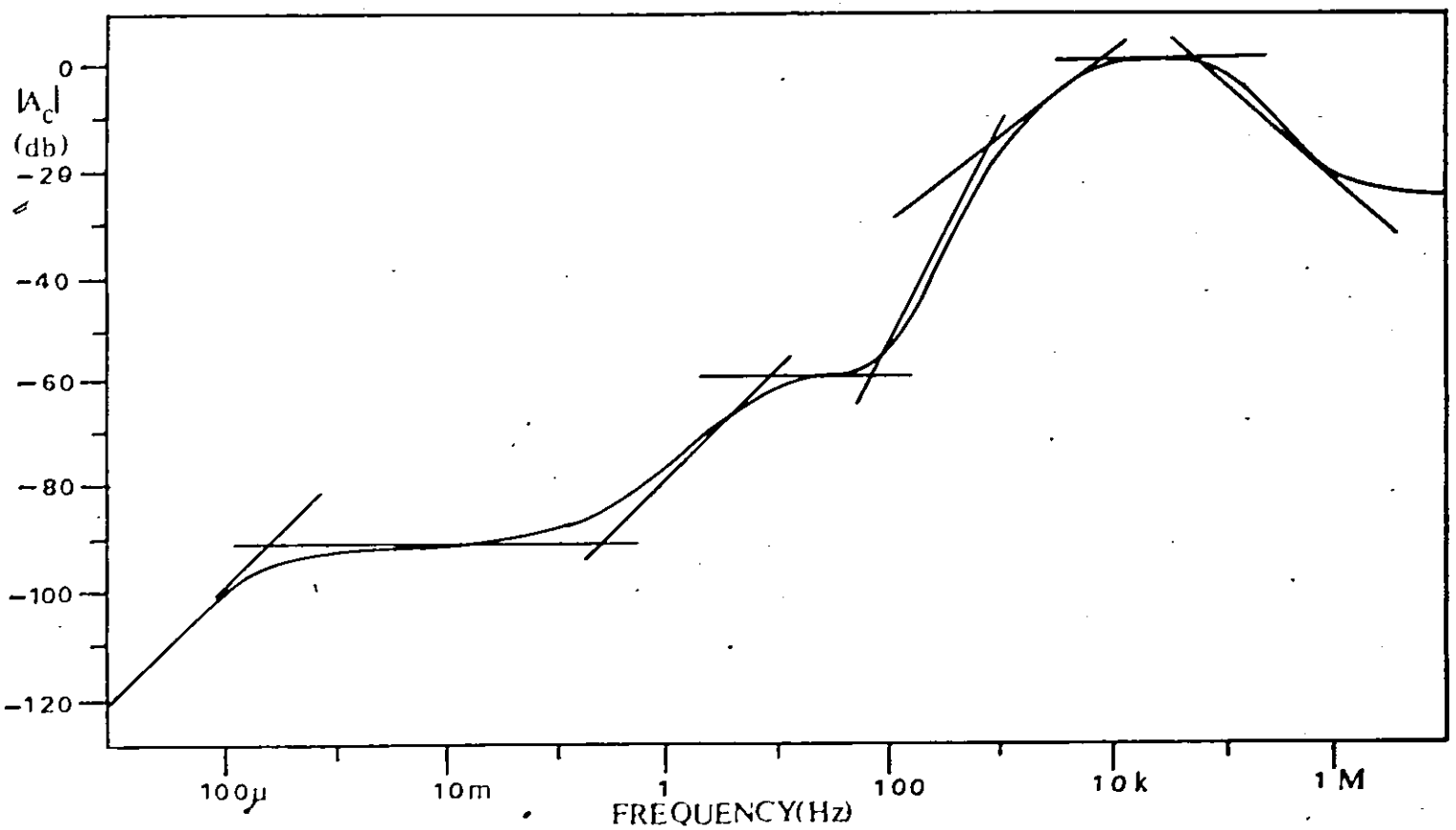

Fig. 2.3 Frequency response of $|A_c|$; theory (asymptote plot) and computer simulation with Z_ℓ parameters , R_ℓ = 10 GΩ, C_ℓ = 100 pF

$$R_L = 8.8\ G\Omega \tag{2.42}$$

$$C_L = 100\ pF \tag{2.43}$$

Z_{cc} is the impedance of an input coupler capacitor of value 0.047 μF, and

$$R_{id} = 1\ M\Omega \tag{2.44}$$

Figure 2.4 shows A_c resulting from computer simulation and experimental data. Since agreement extends over three decades of frequency, both (2.14) and (2.19) are verified as acceptable to at least a first approximation. The slight discrepancies are readily explained by noting that if twenty different differential amplifiers are used, a variation of ±2.5 db is measured.

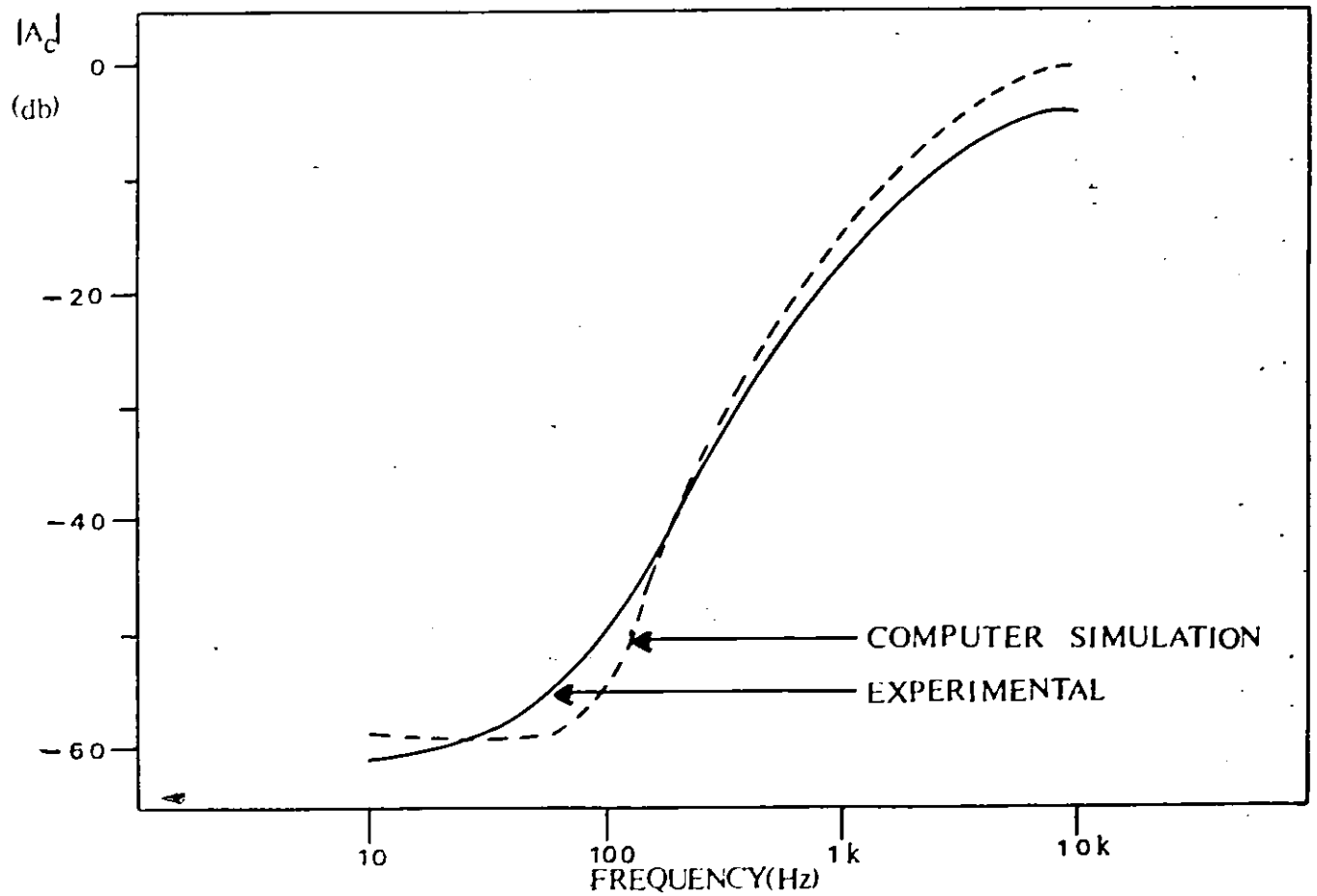

Fig. 2.4 Frequency response of $|A_c|$; experimental data and computer simulation with $\%_2$ parameters, R_2^c = 8.8 GΩ, C_2 = 100 pF

CHAPTER 3

THE EMG AMPLIFIER SYSTEM REQUIREMENTS

3.1 Introduction

Electromyography [4] is defined as the recording of the changes in electrical potential of a muscle, with the myo-electric signals commonly referred to as electromyographic signals or EMG signals. In order to study EMG signals, two things are essential: suitable electrodes to obtain the signal; and some form of signal amplification.

In the first section of this chapter, the various types of electrodes are compared leading to the selection of gold electrodes of area $2cm^2$. The differential amplifier requirement is then determined. A model of the common-mode signal source on a patient leads to the amplifier common-mode gain requirements. The chapter concludes with a summary of the amplifier system specifications required to measure EMG signals.

3.2 Electrode Classification [5]

Electrodes may be extracellular or intracellular. The former have physical dimensions large with respect to muscle cell size and are distant from the cell signal

source. The latter have physical dimensions smaller than the cell dimensions and are placed within the muscle membrane.

EMG studies on medical patients are usually directed at relatively large area muscle motor responses and are not intracellular. Three types of extracellular electrodes exist: needle or fine-wire electrodes inserted below the skin, and surface electrodes. Both needle and fine-wire electrodes have the disadvantage of requiring an experienced person to insert the electrodes into the patient. The popularity of surface electrodes, either wet or dry types, is due to their relative ease of application.

Wet electrodes may be made either disposable or reuseable, and both require careful preparation prior to use. The electrodes are called "wet" because they require the presence of a gel between the electrode material and the skin to form a salt bridge. They are also known as floating junction electrodes. Critical to their proper operation is the salt bridge which has two inherent problems: possible skin reaction to the chemical gel and the drying out of the gel with time.

Dry electrode types have the following advantages over the wet types: 1) a minimum of preparation is required to apply them to the subject since the electrode is applied directly to the skin with no salt bridge; 2) with a proper

choice of electrode material, little if any skin reaction will occur.

3.3 Dry Electrode Considerations

The primary considerations in deciding which electrode material to use are: skin-electrode chemical interaction, muscle motor response area, and the skin-electrode impedance.

Dr. H. deBruin [11] stated that the largest normally used surface EMG electrode is 3.14 cm^2 while the smallest is 0.78 cm^2, the area being a reflection of the typical muscle motor response area to be studied. A compromise value of 2 cm^2 was chosen for the area of a fixed dry electrode.

The question of chemical reaction at the skin-electrode interface is solved by considering only those materials that do not readily react. Two materials known for their inertness to chemical reaction with the skin are gold and stainless steel, with gold having less impedance than stainless steel [7].

Since electrode-skin impedance may vary with increasing current density through the electrode [8], care must be taken when experimentally determining the impedance [9]. To experimentally verify that the impedance measured was not a function of the current density, current levels of 1 μA and 10 μA were used since the electrodes will have less

than 1 μA flowing through them in practice.

Figure 3.1 shows the measured electrode-skin impedance, Z_{skin}, versus frequency for more than one test subject, for gold electrodes of area 2 cm^2.

Since a large EMG signal is 1 mV (pk-pk) for a strong muscle contraction [11], the gain of the EMG amplifier is typically set at 40 db to achieve a good signal-to-noise ratio at the output of the amplifier, and to enable transmission over a suitable distance.

In order to represent the driving point electrode-skin impedance of Fig. 3.1, Z_{skin} will be modelled as a resistor and capacitor in parallel, with parameters R_{skin} = 46 kΩ and C_{skin} = 24 nF. An equivalent circuit model of the EMG source is shown in Fig. 3.2.

3.4 The Differential Amplifier Requirements

The EMG signal frequency spectrum is a function of the center-to-center spacing of the electrodes, with spacings of 1 to 3 cm used typically [11]. For a fixed electrode configuration, a 2.2 cm center-to-center spacing was decided upon, with 95% of the frequency spectrum between 10-250 Hz [11].

It was decided that a differential input impedance of one megaohm was suitable, as this results in an insertion loss of less than 1 db per electrode, a loss which will not

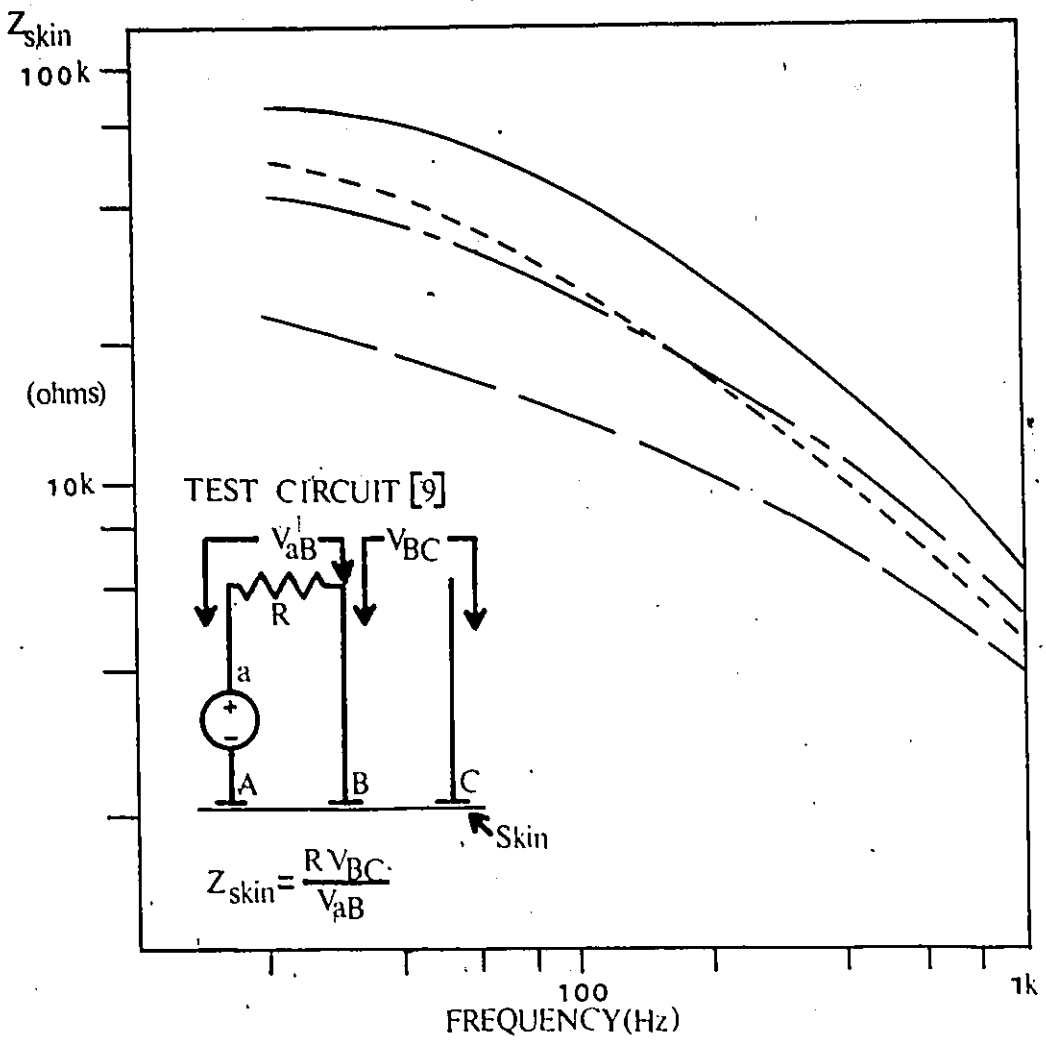

Fig. 3.1 Electrode skin impedance Z_{skin} versus frequency for gold electrodes of area 2 cm^2

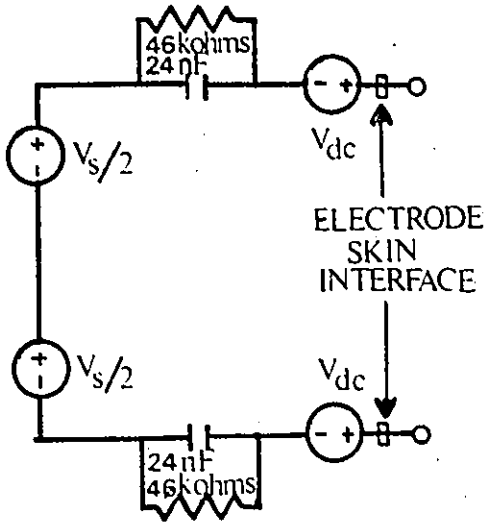

Fig. 3.2 An equivalent circuit model of the EMG source

impair the performance in any manner [11]. Also a high input impedance will minimize the effects of both the variation and mismatch of Z_{skin} on amplifier common-mode performance [2.9].

The differential amplifier must be AC coupled to the electrodes to block DC potentials residing on the skin [12]. A low-frequency filter should also be incorporated in the differential amplifier to minimize the effects of both body motion artifact and wire bounce. A low frequency filter with a -3 db frequency at 8 Hz with a minimum slope of 12 db/octave was suggested [6]. Wire bounce can also be minimized by keeping the distance between the electrodes and the amplifier minimal.

3.5 The Common-Mode Signal

If an electrode is placed on a patient and its output is directly connected to an oscilloscope referenced to system ground, a power-line frequency signal is observed, typically less than 10 V (pk-pk). If a point on the patient is then connected to system ground, the common-mode signal level drops to less than 200 mV (pk-pk). Later, it was demonstrated that the unsymmetrical placement of the system ground connection to the patient, did not significantly affect the observations.

Figure 3.3, is a circuit model proposed to explain

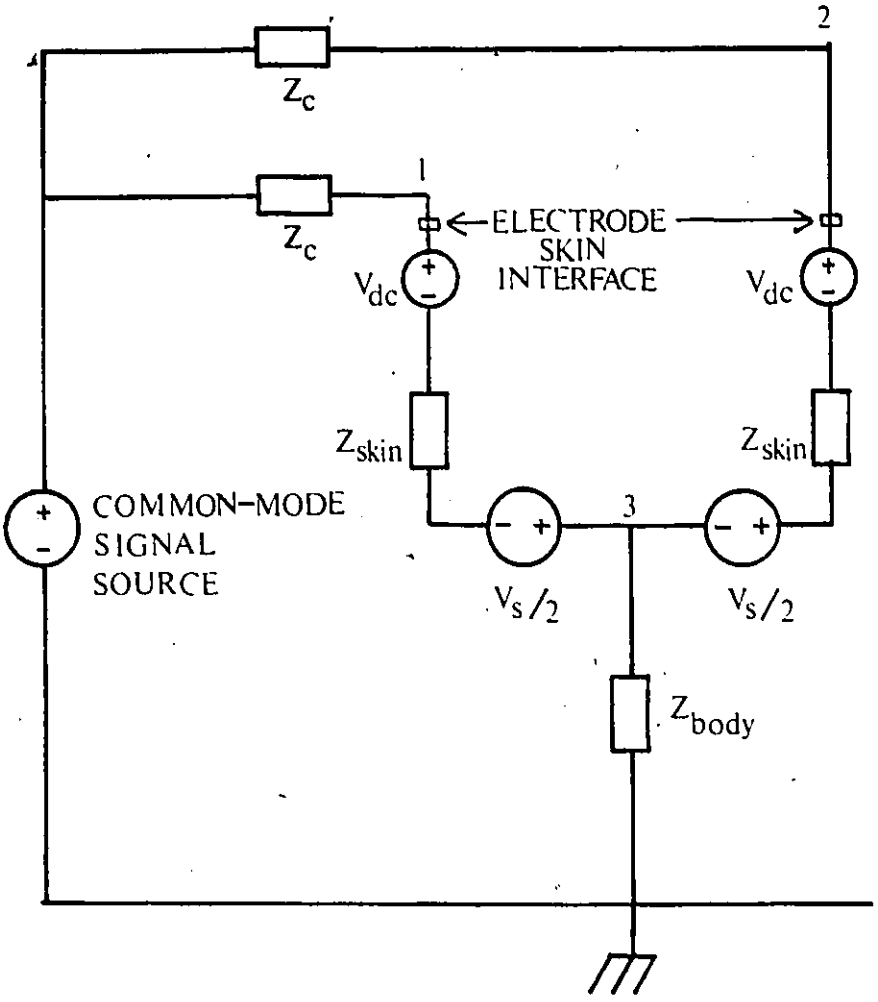

Fig. 3.3 General model of sources

the observations. Z_{body} represents the impedance from the body to system ground and is several times larger than Z_{skin} which is approximately 46 kΩ at 60 Hz for gold electrodes. Z_c represents the coupling impedance from the skin surface to the common-mode signal source, which can be assumed to be the power-line voltage of 110-220 V (rms). For nodes 1 and 2 to have a potential with respect to system ground of a few volts, Z_c must therefore be considerably greater than either Z_{skin} or Z_{body}. The experimental observations can now be explained, for when a point on the skin is placed at system ground potential, Z_{body} is shunted by Z_{skin} and a larger voltage drop occurs across Z_c than before.

The amplifier requirements for common-mode signals is therefore dependent on the existence of a system ground connection to the patient. If no such connection is made, then A_c must be less than -67 db, while if the connection is made an A_c equal to -30 db will suffice. These specifications are arrived at by considering the common-mode gain of a currently used system to measure EMG [10].

3.6 Summary

For the selected electrodes, the amplifier requirements for the measurement of EMG signals are:

1) a bandpass response with a midband gain of 40 db,
2) a second-order low-frequency response with the -3

db frequency point at 8 Hz,

3) a first-order high-frequency response with the -3 db frequency point beyond 250 Hz,

4) a differential amplifier input impedance equal to 1 MΩ.

The amplifier requirements for the common-mode signals are dependant on the existence of a system ground connection to the patient. If no such connection is made, then A_c must be less than -67 db, while if the connection is made an A_c equal to -30 db will suffice.

CHAPTER 4

THE DIFFERENTIAL AMPLIFIER

4.1 Introduction

The differential amplifier configuration is shown in Fig. 4.1, and is a commonly used circuit [2], but for the addition of capacitors C_{a1}, C_{a2}, which are required here to maintain the dc bias circuitry within the two subcircuit amplifiers A_1 and A_2 (Appendix A). This configuration was chosen for the following reasons:

1) only two subcircuit amplifiers are used,
2) no large resistance values are required,
3) the differential gain, A_d, may be easily trimmed by varying G_g, which does not significantly influence A_{cv}.

The subcircuit amplifier is characterized by:

1) a feedback conductance G_2,
2) an input resistance $R_{id}/2$,
3) a finite low-frequency gain A_O,
4) a single pole p_A,
5) two resistors which establish a reference dc biasing current I_C,

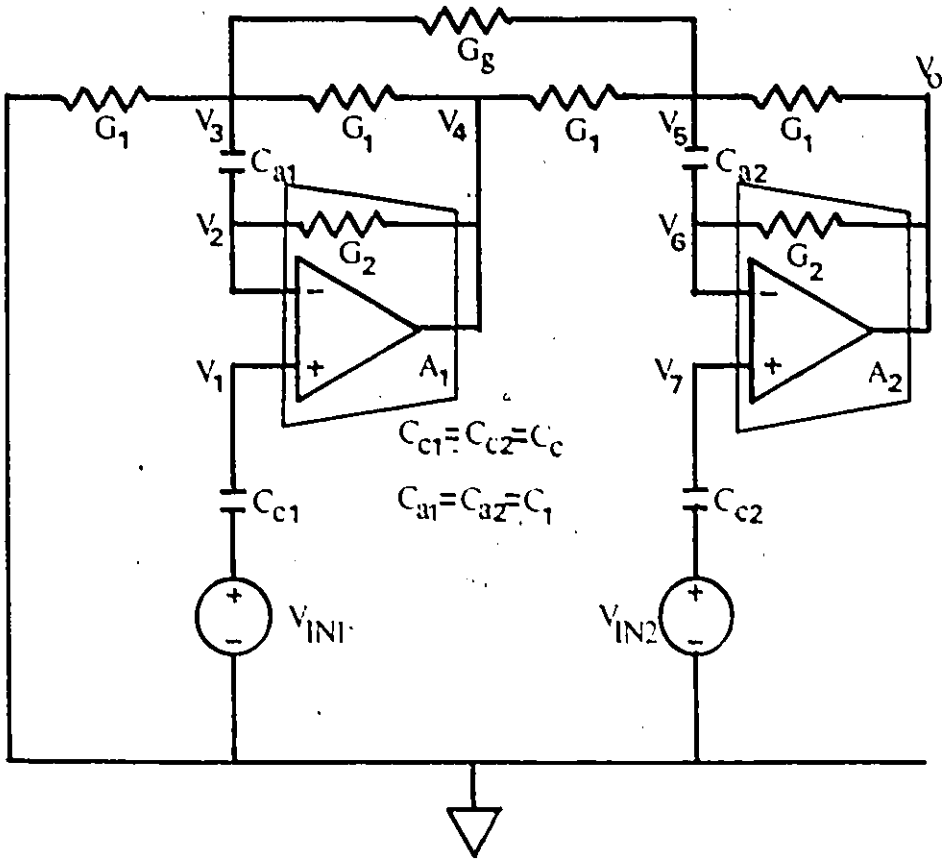

Fig. 4.1 The differential amplifier

6) a resistor R_e that determines the current in the final stage.

A basic simplifying assumption made in the following analysis is that $C_{a1} = C_{a2} = C_1$ and $C_{c1} = C_{c2} = C_c$.

The analysis of the differential amplifier is presented with various simplifications to provide insight into the relationships among circuit parameters, the differential frequency response and the common-mode frequency response. Inspection of Fig. 2.1, shows that four capacitors exist plus two additional capacitors within the two subcircuit amplifiers. Since the amplifier system common-mode response must roll-off at some frequency, the order of the numerator of the transfer function describing A_{cv} must be at least one order less than the denominator, therefore

$$A_{cv} = \frac{(s-z_1)(s-z_2)(s-z_3)(s-z_4)(s-z_5)}{(s-p_1)(s-p_2)(s-p_3)(s-p_4)(s-p_5)(s-p_6)} \qquad (4.1)$$

A complete analysis which included all capacitors would result in a mathematical expression which may not clearly show the dominating factors determining the significant poles and zeros. Therefore, as a simplifying step two frequency ranges for the analysis of the circuit are assumed, a high frequency case where C_1 and C_c may be considered as short circuited and a low frequency case where

the poles associated with the subcircuit amplifiers may be ignored.

In order to further simplify the calculation of the common-mode frequency response, the circuit is considered to be ideal in terms of having no mismatch of components. The only mismatch is due to $sC_1 + G_2$ in parallel with only two of the G_1's.

4.2 The Differential Gain at Low Frequencies

The differential gain, A_d, is calculated by assuming that the subcircuit amplifiers are ideal operational amplifiers and C_c a short circuit. The differential input signal V_s is applied to the non-inverting input of A_1 with the non-inverting input of A_2 grounded.

$$V_s = V_{IN1} = V_1 = V_2 \tag{4.2}$$

$$V_6 = V_7 = V_{IN2} = 0 \tag{4.3}$$

The node-voltage equations are,

$$V_3G_1 + (V_3-V_4)\,G_1 + (V_3-V_5)\,G_g + (V_3-V_2)\,sC_1 = 0 \tag{4.4}$$

$$(V_2-V_3)\,s\,C_1 + (V_2-V_4)\,G_2 = 0 \tag{4.5}$$

$$(V_5-V_4)\,G_1 + (V_5-V_3)\,G_g + (V_5-V_0)\,G_1 + (V_5-V_6)\,sC_1 = 0 \tag{4.6}$$

$$(V_6-V_5)\,sC_1 + (V_6-V_0)\,G_2 = 0 \tag{4.7}$$

The solution may be written as

$$A_{dL} = \frac{V_0}{V_s} = \frac{-s^2C_1^2(G_1+G_g)(G_2+2G_1) - sC_1(2G_1^2G_2+2G_1G_2G_g)}{s^2C_1^2(G_1+G_2)^2 + sC_1[2(G_1+G_2)(2G_1G_2+G_2G_g)+G_1G_2G_g] + (2G_1G_2+G_2G_g)^2 - G_g^2G_2^2} \quad (4.8)$$

which may be rewritten as

$$A_{dL} = -A_{dL0}\frac{s(s-z_{dL1})}{(s-p_{dL1})(s-p_{dL2})} \quad (4.9)$$

with

$$A_{dL0} = 2 + \frac{2G_g}{G_1} \quad (4.10)$$

$$z_{dL1} = -\frac{2G_1^2G_2+2G_1G_2G_g}{C_1(G_1+G_g)(G_2+2G_1)} \quad (4.11)$$

$$p_{dL1} = -\frac{2(G_1+G_2)(2G_1G_2+G_2G_g)+G_1G_2G_g}{C_1(G_1+G_2)^2} \quad (4.12)$$

$$p_{dL2} = -\frac{(2G_1G_2+G_2G_g)^2-G_g^2G_2^2}{C_1[2(G_1+G_2)(2G_1G_2+G_2G_g)+G_1G_2G_g]} \quad (4.13)$$

An approximation to the midband differential gain is made so that later it may be substituted into other equations thereby providing insight into various functional relationships.

$$A_d = \frac{2G_g}{G_1} \quad (4.14)$$

The effect on A_d of capacitor C_c is now included by using a simple voltage divider relation

$$V_1 = V_2 = V_{IN1} = V_s \frac{R_{id}/2}{R_{id}/2 + 1/sC_c} \tag{4.15}$$

which introduces an additional pole and zero into (4.9). Thus

$$A_{dL} = \frac{sK_{dL}}{s-p_{dL3}} A_{dL0} \frac{s(s-z_{dL1})}{(s-p_{dL1})(s-p_{dL2})} \tag{4.16}$$

with

$$K_{dL} = C_{c1}/G_{id} \tag{4.17}$$

$$p_{dL3} = -2\ G_{id}/C_{L1} \tag{4.18}$$

Since the differential gain is to be 40 db, the values of R_1 and R_g are chosen to be equal to 10 kΩ and 200 Ω respectively. It can be seen that p_{dL2} is much less than p_{dL1}. To set the low-frequency -3 db point at 8 Hz, and have the two poles p_{dL2} and p_{dL3} equal, the values of C_c and C_1 are chosen to be 0.047 μF / 7 μF respectively.

4.3 The High-Frequency Differential Gain

At high frequencies, C_1 and C_c can be considered to be short circuits. In this frequency range the subcircuit amplifiers are modelled as finite-gain single-pole voltage amplifiers but are otherwise ideal. The following mathematical notation is used

$$s_1 = s/(-p_{A1}) \tag{4.19}$$

$$s_2 = s/(-p_{A2}) \tag{4.20}$$

The equations describing the non-ideal behaviour of the subcircuit amplifiers are then

$$V_4 = \frac{A_{O1}(V_1-V_2)}{(1+s_1)} \tag{4.21}$$

$$V_0 = \frac{A_{O2}(V_7-V_6)}{(1+s_2)} \tag{4.22}$$

For simplification

$$G_2 = 0 \tag{4.23}$$

Inspection shows that

$$V_{IN2} = V_7 = 0 \tag{4.24}$$

$$V_{IN1} = V_1 = V_s \tag{4.25}$$

$$V_3 = V_2 \tag{4.26}$$

$$V_5 = V_6 \tag{4.27}$$

The node-voltage equatons are,

$$V_3 G_1 + (V_3-V_4) G_1 + (V_3-V_5) G_g = 0 \tag{4.28}$$

$$(V_5-V_4) G_1 + (V_5-V_3) G_g + (V_5-V_0) G_1 = 0 \tag{4.29}$$

The solution may be written

$$A_{dH} = \frac{V_0}{V_s} = \frac{-1}{\frac{2s_1s_2}{A_{O1}A_{O2}} + \frac{s_2}{A_{O2}} + \frac{s_1(2G_1+G_g)}{A_{O1}(2G_1+2G_g)} + \frac{1}{A_d}} \tag{4.30}$$

which may be rewritten as

$$A_{dH} = \frac{-1}{(s-p_{dH1})(s-p_{dH2})} \tag{4.31}$$

where

$$P_{dH1} = \frac{A_{O1}P_{A1}}{2} + \frac{(2G_1+G_g)}{(2G_1+2G_g)} \frac{A_{O2}P_{A2}}{2} \tag{4.32}$$

$$P_{dH2} = \frac{A_{O2}P_{A2}A_{O1}P_{A1}(2G_1+2G_g)}{A_d[A_{O1}P_{A1}(2G_1+2G_g)+A_{O2}P_{A2}(2G_1+G_g)} \tag{4.33}$$

4.4 The Overall Differential Gain Frequency Response

The differential gain may be asymptotically plotted using (4.16) for low frequencies and (4.31) for high frequencies. Figure 4.2 shows the asymptotic plot and computer simulation results, which are in good agreement for the following three different bias conditions in the subcircuit amplifiers:

1) $I_{C1} = I_{C2} = 2.8$ μA,

2) $I_{C1} = 10$ μA and $I_{C2} = 2.8$ μA,

3) $I_{C1} = I_{C2} = 10$ μA.

4.5 The Common-Mode Gain Response at High Frequencies

The common-mode input signal V_{cm} is applied to the non-inverting terminals. At high frequencies C_c and C_1 can be considered as short circuits and the subcircuit amplifiers are modelled as finite-gain single-pole voltage amplifiers as in (4.21) and (4.22). Let

$$G_3 = G_1 + G_2 \tag{4.34}$$

Inspection shows that

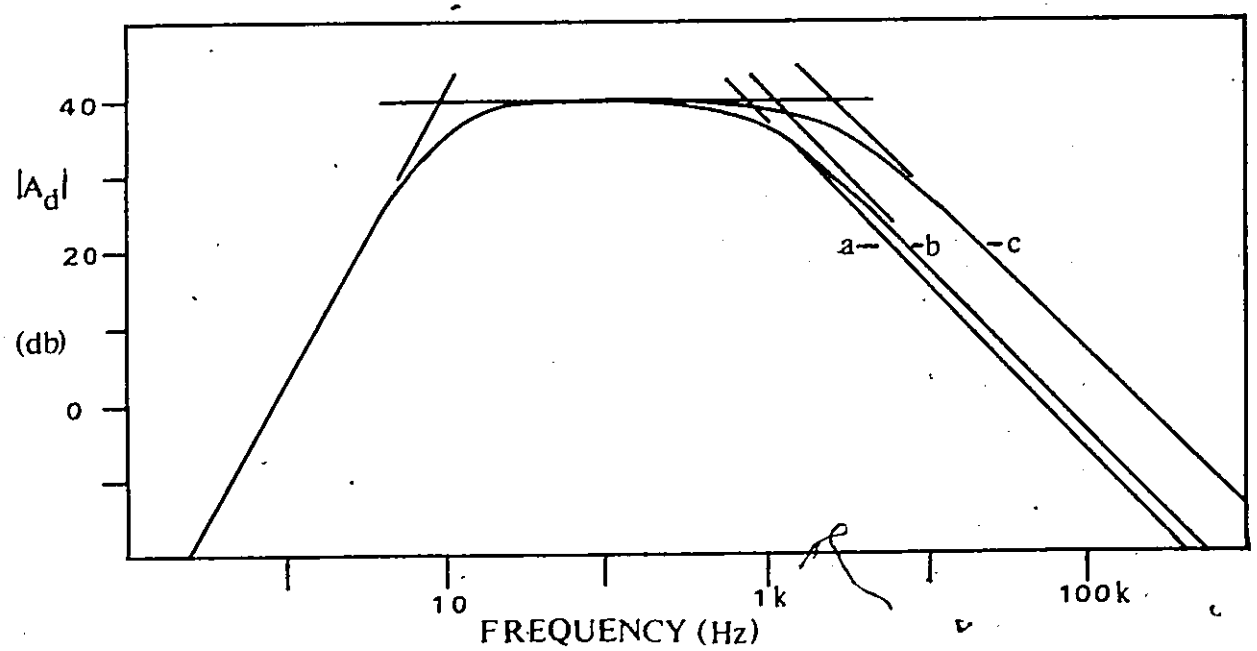

Fig. 4.2 Differential gain frequency response $|A_d|$,

(a) Equal bias in A_1 and A_2, I_C= 2.8 μA

(b) Unequal bias in A_1 and A_2, I_{C1}= 10 μA, I_{C2}= 2.8 μA

(c) Equal bias in A_1 and A_2, I_C= 10 μA

$$V_{cm} = V_{IN1} = V_{IN2} = V_1 = V_7 \tag{4.35}$$

$$V_2 = V_3 \tag{4.36}$$

$$V_5 = V_6 \tag{4.37}$$

Node-voltage analysis yields,

$$V_3 G_1 + (V_3-V_4) G_3 + (V_3-V_5) G_g = 0 \tag{4.38}$$

$$(V_5-V_4) G_1 + (V_5-V_3) G_g + (V_5-V_0) G_3 = 0 \tag{4.39}$$

The solution is

$$A_{cvH} = \frac{V_0}{V_{cm}} = \frac{\begin{array}{l} s_1 A_{O2} (G_1+G_3) (G_1+G_3+2G_g) \\ +A_{O2} (G_1+G_3) (G_1+G_3+2G_g) + A_{O1} A_{O2} (G_3^2-G_1^2) \end{array}}{\begin{array}{l} s_1 s_2 [(G_1+G_3)^2+2G_g (G_1+G_3)] \\ +s_1 [(G_1+G_3)^2+2G_g (G_1+G_3)+A_{O2} G_3 (G_1+G_3+G_g)] \\ +s_2 [(G_1+G_3)^2+2G_g (G_1+G_3)+A_{O1} G_1 G_g+A_{O1} G_3 (G_1+G_3+G_g)] \\ +(G_1+G_3)^2+2G_g (G_1+G_3)+A_{O1} A_{O2} G_3^2+A_{O1} G_1 G_g \\ +(A_{O2} G_3+A_{O1} G_3) (G_1+G_3+G_g) \end{array}} \tag{4.40}$$

which may be rewritten as

$$A_{cvH} = \frac{V_0}{V_{cm}} = A_{cvHo} \frac{(s-z_{cH1})}{(s-p_{cH1})(s-p_{cH2})} \tag{4.41}$$

where

$$A_{cvHo} = \frac{2A_d}{A_{O1}} + 1 - \frac{G_1^2}{G_3^2} \tag{4.42}$$

and

$$z_{cH1} = - p_{A1} + \frac{p_{A1}(G_3^2-G_1^2)}{A_{O2}(G_1+G_3)(G_1+G_3+2G_g)} \qquad (4.43)$$

If

$$G_1 = G_3 \qquad (4.44)$$

Then,

$$p_{cH1} = - [\frac{p_{A1}A_{01}}{2} + \frac{p_{A2}A_{02}}{4}] \qquad (4.45)$$

$$p_{cH2} = - \frac{p_{A1}p_{A2}\ [A_{02} + 2A_{01} + \frac{2A_{01}A_{02}}{A_d}]}{A_{02}\ p_{A2} + 2\ A_{01}\ p_{A1}} \qquad (4.46)$$

A_{cvH} is plotted asymptotically in Fig. 4.3(a) for the case of subcircuit amplifiers A_1 and A_2 equally biased with I_C = 2.8 μA, R_{e1} = 10 kΩ, and R_{e2} = 1.8 kΩ. The rise in A_{cvH} is due to z_{cH1} which is primarily a function of the single pole p_{A1} of A_1. These results suggest that an improvement in A_{cvH} is thus possible by either reducing the compensation capacitor and/or increasing I_{C1} to move the pole p_{A1} to a higher frequency.

4.6 The Common-Mode Gain Response at Low Frequencies

This low-frequency analysis differs from the previous case in that C_1 is not considered to be a short circuit, and it is assumed that the subcircuit amplifiers may be modelled as ideal voltage amplifiers. C_c is considered to be short circuited initially. Then by inspection,

a)

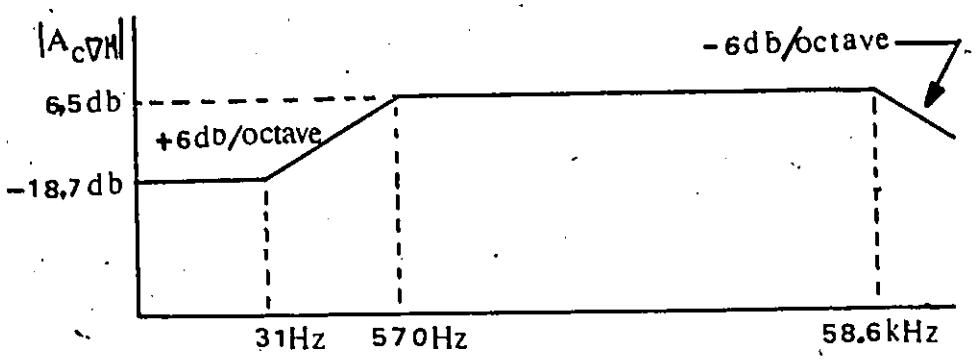

b)

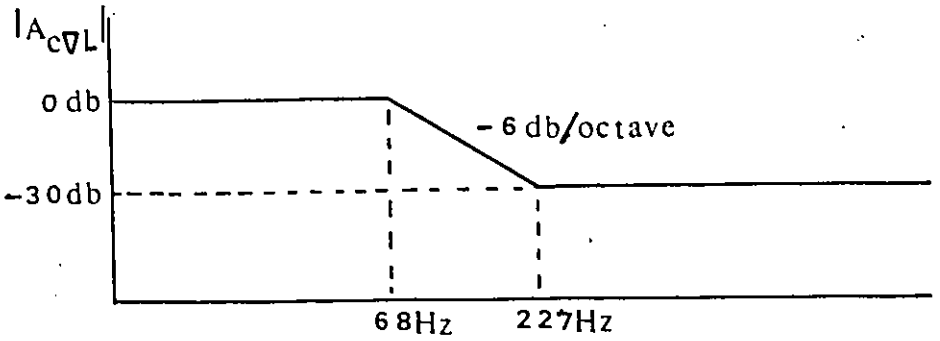

Fig. 4.3 Frequency response of $|A_{cv}|$, asymptotically plotted

(a) High-frequency case

(b) Low-frequency case

$$V_{cm} = V_1 = V_2 = V_6 = V_7 \tag{4.47}$$

The node-voltage equations are,

$$(V_2-V_3)\ sC_1 + (V_2-V_4)\ G_2 = 0 \tag{4.48}$$

$$V_3\ G_1 + (V_3-V_4)\ G_1 + (V_3-V_5)\ G_g = 0 \tag{4.49}$$

$$(V_5-V_4)\ G_1 + (V_5-V_3)\ G_g + (V_5-V_0)\ G_1 + (V_5-V_6)\ sC_1 = 0 \tag{4.50}$$

$$(V_6-V_5)\ sC_1 + (V_6-V_0)\ G_2 = 0 \tag{4.51}$$

The solution may be written as

$$A_{cvL} = \frac{V_0}{V_{cm}} =$$

$$\frac{s^2C_1^2G_2(2G_1+G_2)+sC_1G_2[4G_1(G_1+G_2)+2G_g(2G_1+G_2)]+4G_1G_2(G_1+G_g)}{s^2C_1^2(G_2+G_1)^2+sC_1G_2[(2G_2+2G_1)(G_g+2G_1)+G_gG_1]+4G_1G_2(G_1+G_g)} \tag{4.52}$$

which may be rewritten as,

$$A_{cvL} = \frac{V_0}{V_{cm}} = A_{cvLo}\ \frac{(\frac{s}{z_{cL1}} - 1)(\frac{s}{z_{cL2}} - 1)}{(\frac{s}{p_{cL1}} - 1)(\frac{s}{p_{cL2}} - 1)} \tag{4.53}$$

where

$$A_{cvLo} = 1 \tag{4.54}$$

$$z_{cL1} = -\frac{G_2[4G_1(G_1+G_2)+2G_g(2G_1+G_2)]}{C_1\ G_2\ (2G_1 + G_2)} \tag{4.55}$$

$$z_{cL2} = \frac{-4\ G_1\ G_2\ (G_1 + G_g)}{C_1G_2[4G_1(G_1+G_2)+2G_g(2G_1+G_2)]} \tag{4.56}$$

$$p_{cL1} = \frac{-G_2[(2G_2+2G_1)(G_g+2G_1)+G_gG_1]}{C_1(G_2+G_1)^2} \tag{4.57}$$

$$p_{cL2} = \frac{-4\,G_1\,G_2\,(G_1+G_g)}{C_1G_2[(2G_2+2G_1)(G_g+2G_1)+G_gG_1]} \tag{4.58}$$

If

$$G_2 << G_1, \tag{4.59}$$

Then z_{cL1} and p_{cL2} are beyond the frequency range of the assumptions made concerning the subcircuit amplifiers and are ignored in the asymptotic plot of A_{cvL} as shown in Fig. 4.3(b).

4.7 The Overall Common-Mode Gain Frequency Response

The common-mode A_{cv} is given for low frequencies by (4.53) and at high frequencies by (4.41), which may be expressed as

$$A_{cv} = \begin{cases} A_{cvLo}\,\dfrac{(s/z_{cL1}-1)(s/z_{cL2}-1)}{(s/p_{cL1}-1)(s/p_{cL2}-1)} & \text{For L.F.} \\ A_{cvHo}\,\dfrac{(s-z_{cH1})}{(s-p_{cH1})(s-p_{cH2})} & \text{For H.F.} \end{cases} \tag{4.60}$$

The effect on Ac_v of capacitor C_c is now included by using a simple voltage divider relation

$$V_{IN1} = V_{IN2} = V_1 = V_2 = V_{cm}\,\frac{R_{id}/2}{R_{id}/2 + 1/sC_c} \tag{4.61}$$

which introduces an additional pole and zero into (4.6). Thus,

$$A_{cv} = \begin{cases} \left(\frac{K_{co}}{s-p_{co}}\right) A_{cvLo} \dfrac{(s/z_{cL1} - 1)(s/z_{cL2} - 1)}{(s/p_{cL1} - 1)(s/p_{cL2} - 1)} & \text{For L.F.} \\ \left(\frac{K_{co}}{s-p_{co}}\right) A_{cvHo} \dfrac{(s-z_{cH1})}{(s-p_{cH1})(s-p_{cH2})} & \text{For H.F.} \end{cases} \tag{4.62}$$

where

$$K_{co} = R_{id} \tag{4.63}$$

$$p_{co} = -2\, G_{id}/C_c \tag{4.64}$$

An asymptotic plot of A_{cv} is shown in Fig. 4.4 along with the computer simulation results, for the case of I_C = 2.8 μA for both A_1 and A_2, R_{e1} = 10 kΩ and R_{e2} = 1.8 kΩ. The differences in the graphs are only in magnitude not shape, and the differences can be explained as arising from the simplifying assumptions made in both the high-frequency and low-frequency analyses. In the high-frequency analysis, the assumption was made that C_1 may be considered a short circuit. Yet with z_{cH1} at 31 Hz, at this frequency the impedance of C_c is 733 Ω which is 7% of G_1. In the low frequency case, the subcircuit amplifier was assumed to be ideal, but p_{cL1} is at a frequency greater than the single pole of the subcircuit amplifier, p_{A1}.

Even with these assumptions introducing some error, there is fair agreement in Fig. 4.4, showing that the dominating poles and zeros are correctly given by (4.62).

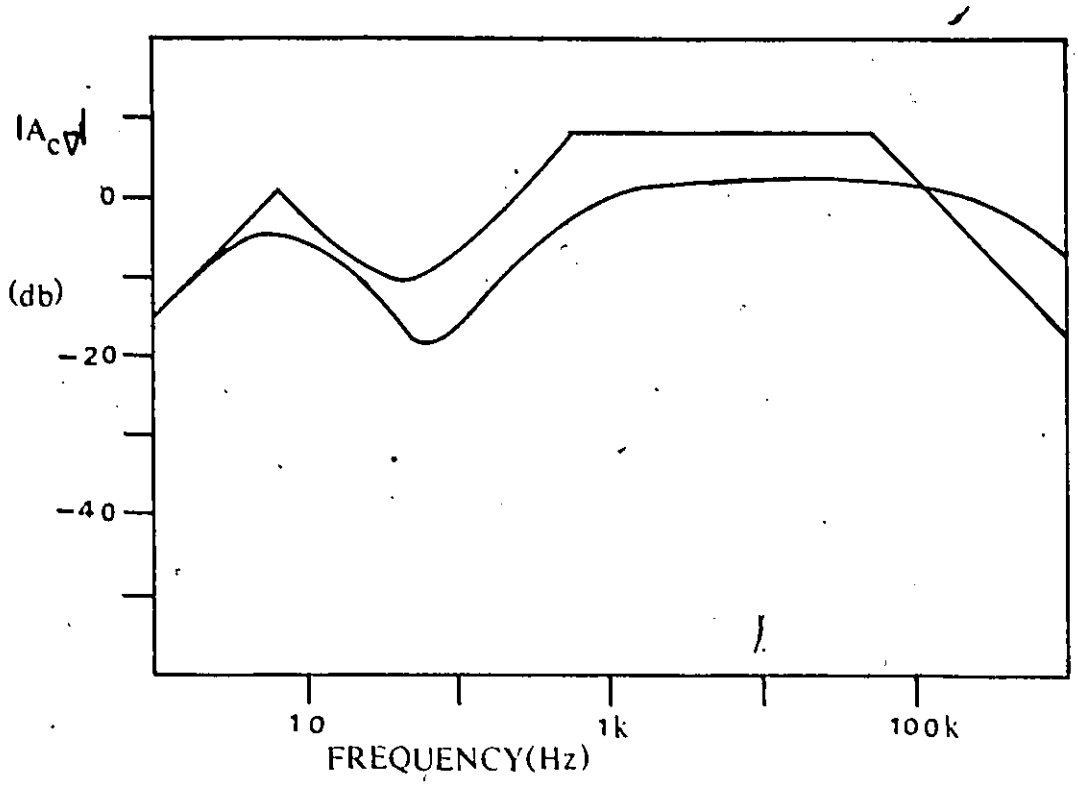

Fig. 4.4 Frequency response of $|A_{cv}|$; theory (asymptotically plotted) and computer simulation results

Reviewing the results, it is seen that the poles and zeros, besides being a function of the element parameters, are also functions of the non-ideal properties of the subcircuit amplifiers, p_A and A_O.

Computer and experimental results are in good agreement as shown in Fig. 4.5 and Fig. 4.6 respectively, for three different subcircuit amplifier biasing cases:

1) $I_{C1} = I_{C2} = 2.8$ μA

2) $I_{C1} = I_{C2} = 10$ μA

3) $I_{C1} = 10$ μA and $I_{C2} = 2.8$ μA

Increasing I_C results in a lower common-mode gain, A_{cv} as was indicated by (4.43), (4.45) and (4.46). The experimental results were taken to one frequency decade beyond any expected differential signal. The small differences between computer and experimental results can be explained by noting that if twenty different subcircuit amplifiers are substituted for either A_1 or A_2, a variation of ±2.5 db is measured.

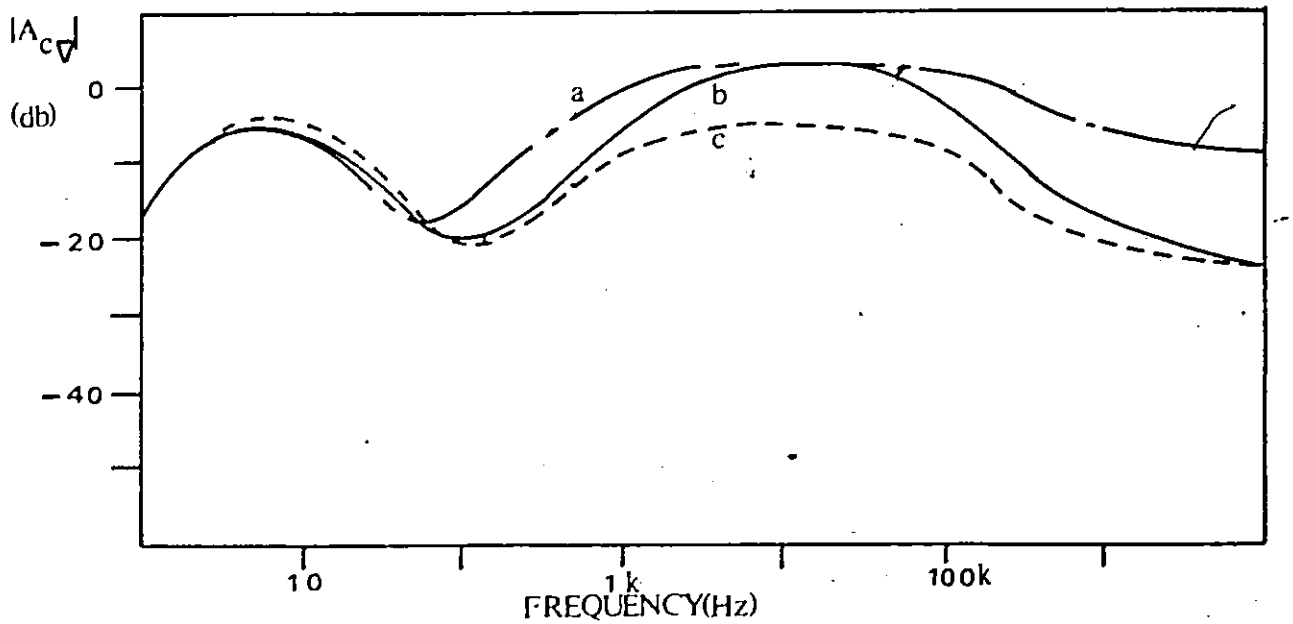

Fig. 4.5 Frequency response of $|A_{cv}|$; computer simulation results for three different subcircuit amplifier bias conditions

(a) Equal bias in A_1 and A_2, I_C= 2.8 μA

(b) Equal bias in A_1 and A_2, I_C= 10 μA

(c) Unequal bias in A_1 and A_2, I_{C2}=2.8 μA, I_{c1}=10μA

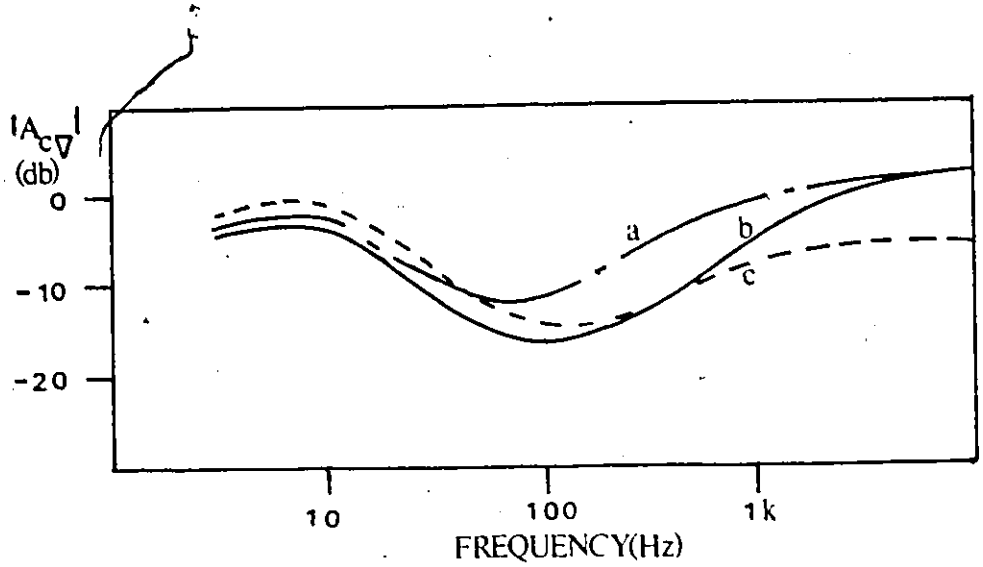

Fig. 4.6 Frequency response of $|A_{c\nabla}|$; experimental results for three different subcircuit amplifier bias conditions

(a) Equal bias in A_1 and A_2, I_C= 2.8μA

(b) Equal bias in A_1 and A_2, I_C= 10μA

(c) Unequal bias in A_1 and A_2, I_{C2}=2.8μA, I_{C1}=10μA

CHAPTER 5

THE EMG AMPLIFIER SYSTEM

5.1 Introduction

The objective of this chapter is to use the information of the previous chapters to design an amplifier system for the measurement of myo-electric signals. The approach taken to reduce the effects of unwanted common-mode signals is to use an output coupler device in conjunction with a differential amplifier.

The output coupler device is assumed to have a frequency independent transfer function of unity magnitude. The overall differential gain of the amplifier system is then due solely to the bandpass frequency response characteristics of the differential amplifier:

1) a mid-band gain of 40 db (4.10),
2) a lower -3 db frequency point at 8 Hz with a slope of -12 db/octave (4.16),
3) an upper -3 db frequency point at 1 kHz with a slope of -6 db/octave (4.31).

It has been shown that the overall common-mode gain A_c can be expressed as the product of the differential

amplifier common-mode gain A_{cv} (4.60), and the isolation gain A_I, (2.20). The isolation gain depends on:

1) the isolation impedance $Z_\ell = [G_\ell + sC_\ell]^{-1}$, which characterizes the common-mode isolation properties of the output coupler device,
2) the differential amplifier input impedance Z_{id} which is equal to 1 MΩ.
3) the impedance Z_{cc} of the input coupler capacitor C_c of value 0.047 μF,
4) the impedance of the differential signal source, Z_{skin}, which is modelled by 46 kΩ in parallel with 24 nF as shown in Fig. 3.2.

The chapter begins with an investigation of the limitations to the minimization of A_I imposed by a finite Z_ℓ. It is shown for the case where R_ℓ is equal to 10 GΩ, that if C_ℓ is greater than 1 pF, then the limitation on the reduction of A_I and hence A_c is determined by C_ℓ at frequencies in excess of 40 Hz. A simple modification of Z_{id} is proposed, which further minimizes A_I and hence A_c.

The chapter concludes with a presentation of an amplifier system design which incorporates both the Z_{id} modification and the unequal dc biasing of the subcircuit amplifiers to achieve a reduction of A_c. The resulting amplifier system exhibits properties which are within the

specifications presented in Chapter Three for the case where a ground lead is connected to the patient. Experimental EMG measurements are presented for the case where the output coupler device is a transformer.

5.2 The Dependence of A_I on the Output Coupler Device Isolation Impedance Z_ℓ

This section will investigate the limitations to the reduction of A_c as imposed by a finite Z_ℓ, under the following conditions:

1) the differential amplifier subcircuit amplifiers are equally biased with I_C = 2.8 μA,
2) R_{e1} = 10 kΩ and R_{e2} = 1.8 kΩ.

Figure 5.1 shows the computer simulation of $|A_c|$ versus frequency with C_ℓ equal to zero, and R_ℓ as a parameter.

Figure 5.2 shows the computer simulation of $|A_c|$ versus frequency with R_ℓ equal to 10 GΩ, and C_ℓ as a parameter.

Figure 5.3 shows the computer simulation of $|A_c|$ versus frequency with both R_ℓ and C_ℓ as parameters.

Experimental data was obtained by isolating the differential amplifier using teflon standoffs between local ground and system ground, and introducing fixed resistors and capacitors to simulate the imperfect isolation

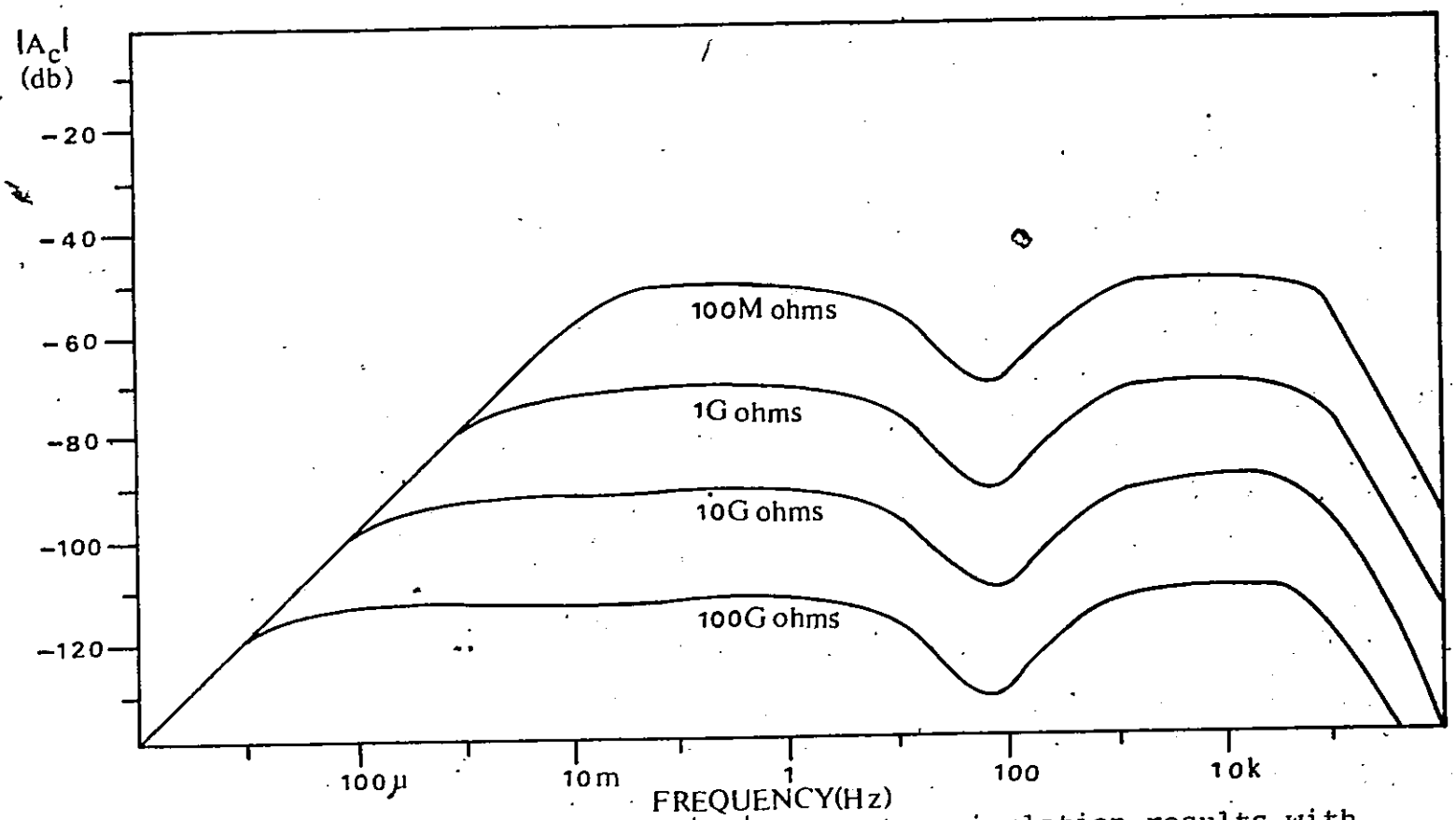

Fig. 5.1 Frequency response of $|A_c|$; computer simulation results with 100 MΩ $\leq R_\ell \leq$ 100 GΩ and $C_\ell = 0$ pF

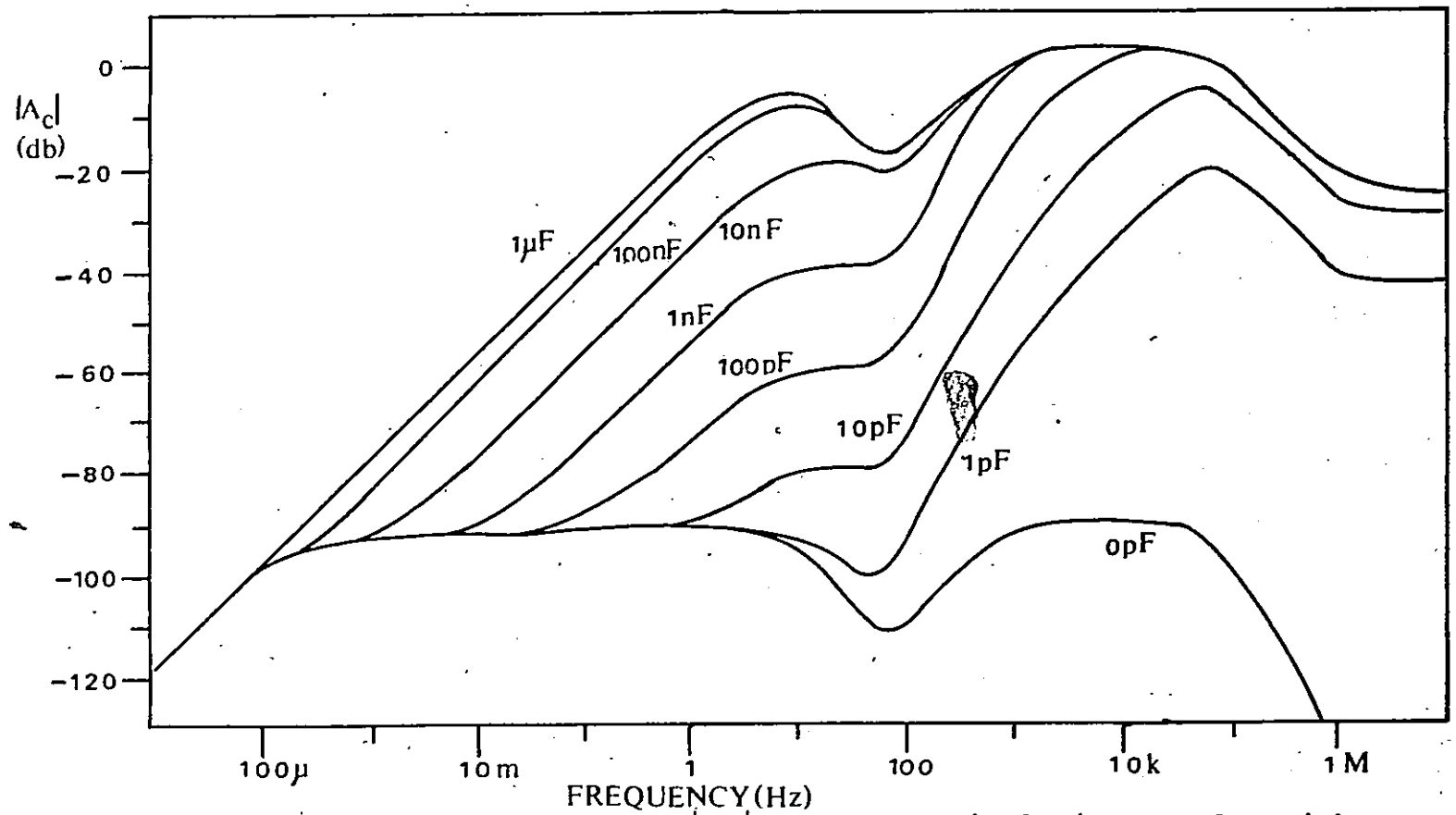

Fig. 5.2 Frequency response of $|A_c|$; computer simulation results with $0\ pF \leq C_\ell \leq 1\ \mu F$ and $R_\ell \cong 10\ G\Omega$

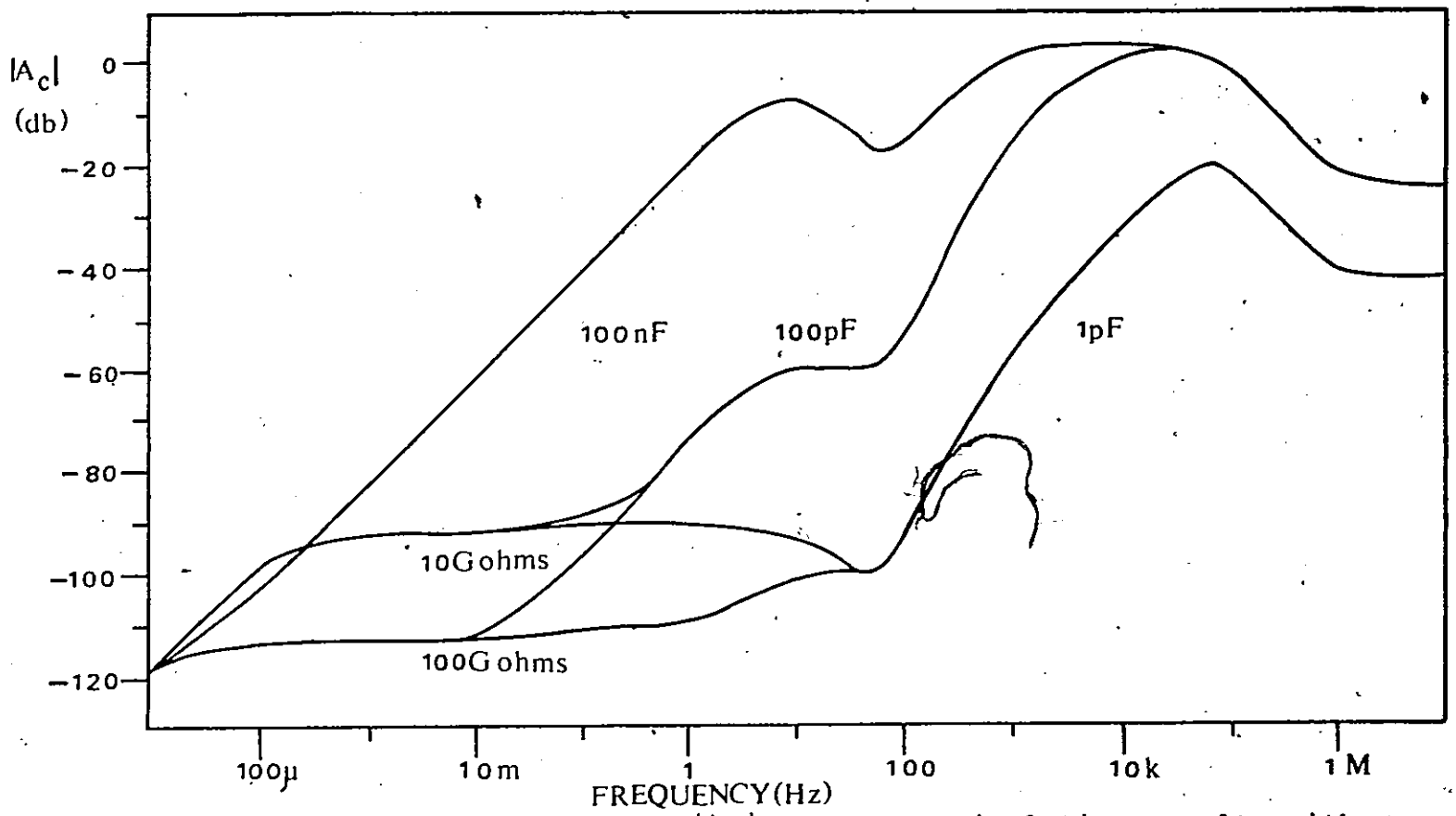

Fig. 5.3 Frequency response of $|A_c|$; computer simulation results with both R_ℓ and C_ℓ as parameters

properties as shown in Fig. 5.4 of an output coupler device. It can be deduced from the data that the effect of stray capacitance is similar to introducing a leakage capacitance of 10-20 pF.

These results show that if R_ℓ is equal to 10 GΩ, that if C_ℓ is greater than 1 pF, then the limitation in the reduction of A_I and hence A_c, is determined by C_ℓ at frequencies in excess of 40 Hz.

The rise in A_I and hence A_c with frequency can be explained with the help of (2.19), for while Z_ℓ decreases with increasing frequency, Z_{id} remains constant. If Z_{id} is made a function similar to Z_ℓ then A_c will be less sensitive to frequency.

The amplifier input impedance, Z_{id} is now modified by placing in parallel to it a capacitor C_{id} as shown in Fig. 5.5. If C_{id} is chosen such that the resulting amplifier input impedance has the same time constant as Z_{skin}, the transfer function from the EMG source to the differential amplifier input terminals will be frequency independent.

The computer simulation results in Fig. 5.6 show a significant improvement in A_c when C_{id} = 1.5 nF. When the model of the electrode-skin impedance of Chapter Three is used, this modification to Z_{id} does not significantly affect A_d as shown in Fig. 5.7.

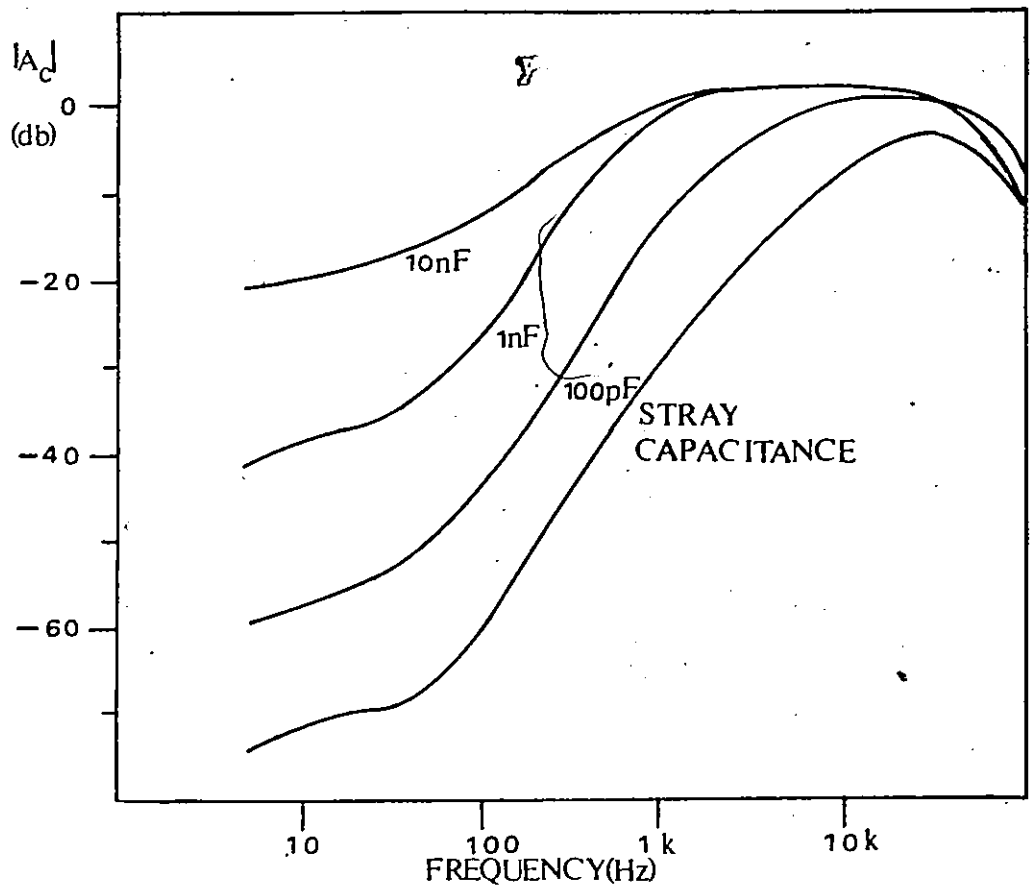

Fig. 5.4 Frequency response of $|A_c|$; experimental results with 0 pf $\leq C_\ell \leq$ 10 nF and R_ℓ=10 GΩ

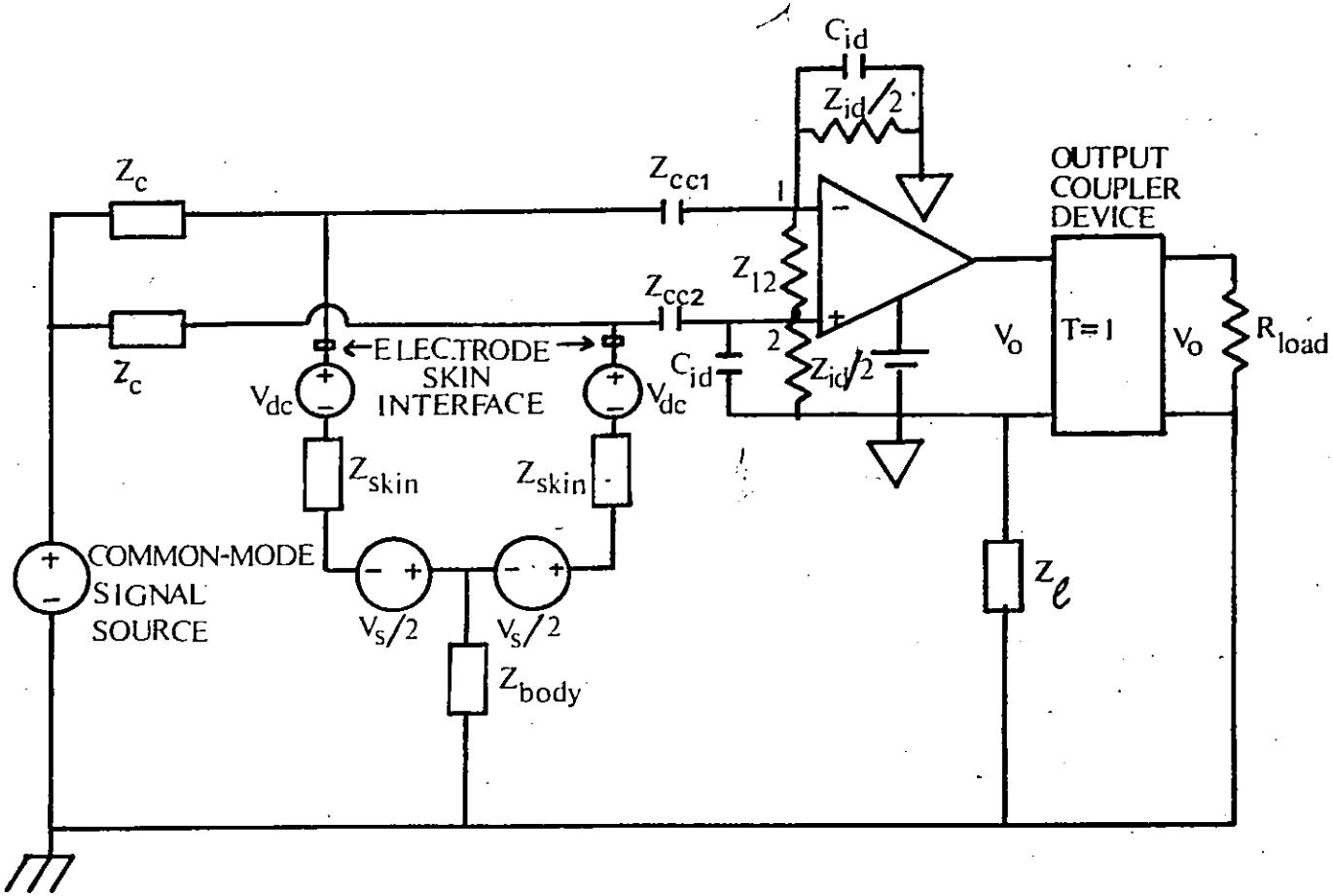

Fig. 5.5 General system model of amplifier to measure EMG with Z_{id} modification shown

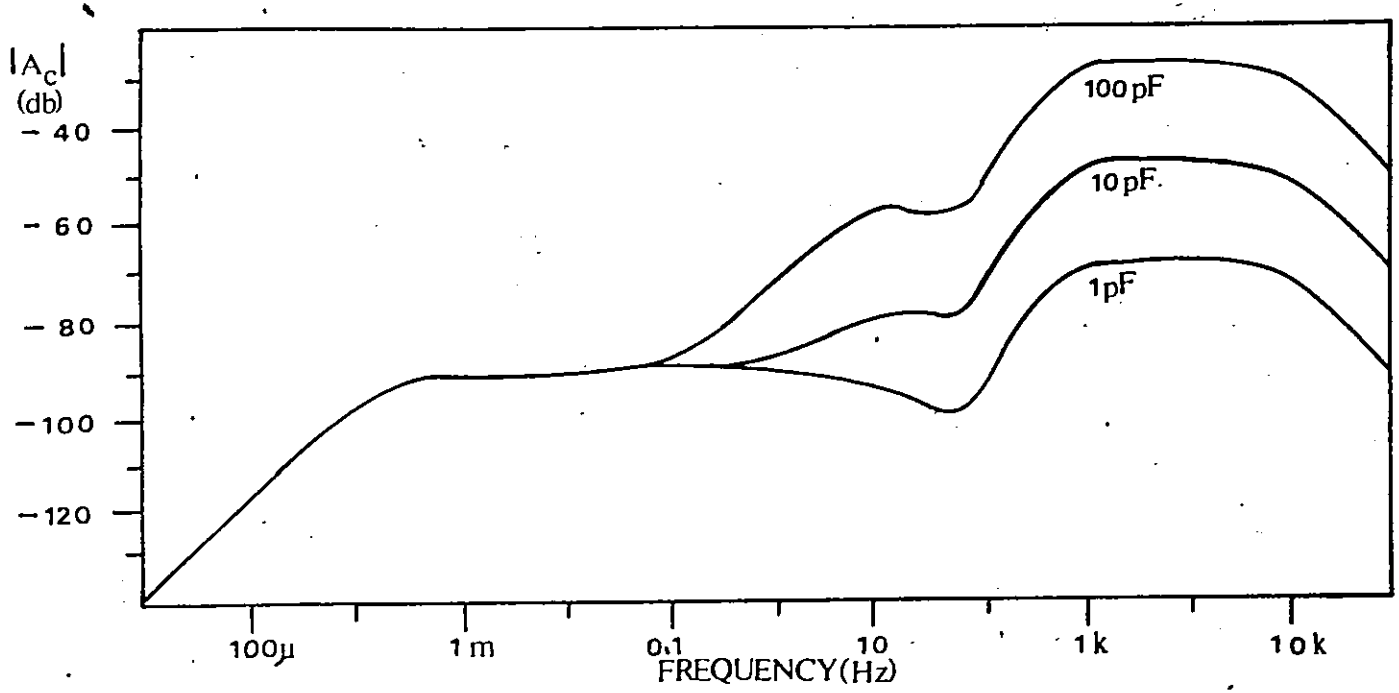

Fig. 5.6 Frequency response of $|A_c|$; computer simulation results with Z_{id} modification (C^c_{id}= 1.5 nF)

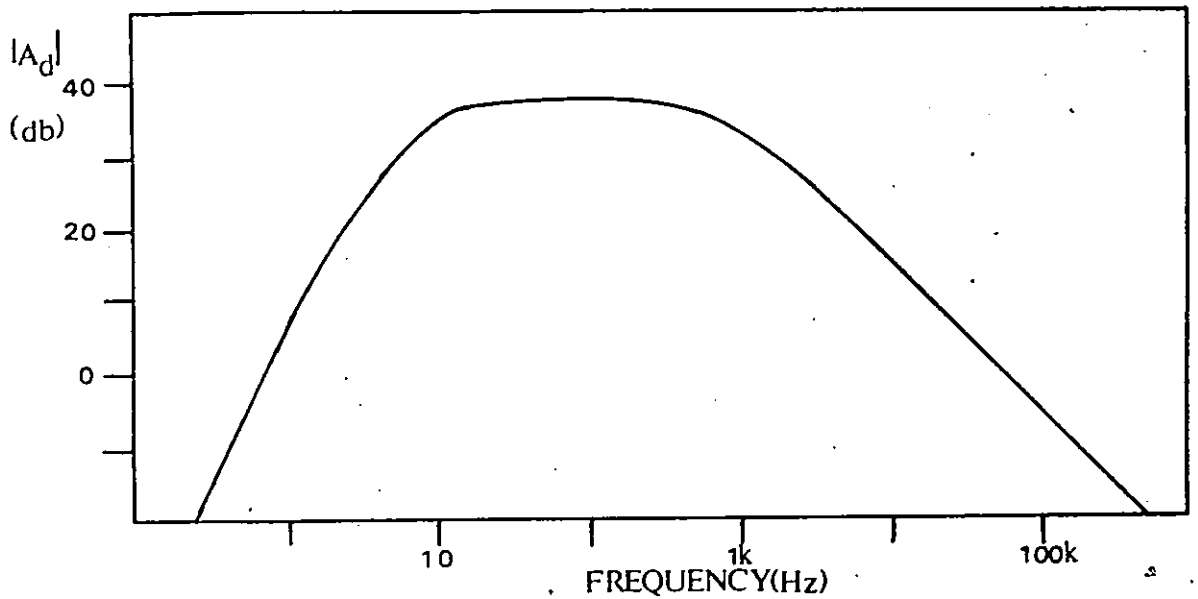

Fig. 5.7 Frequency response of $|A_d|$; computer simulation results using an EMG differential source (Fig. 3.2) with Z_{id} modification (C_{id}= 1.5 nF)

5.3 The Overall Performance of the EMG Amplifier System Design

This section presents the overall performance of an amplifier system designed to measure EMG using both the Z_{id} modification and unequal dc biasing of the subcircuit amplifiers to minimize A_c, i.e. I_{C1} = 10 μA, I_{C2} = 2.8 μA.

The performance of this amplifier system was tested using computer simulation with R_ℓ equal to 10 GΩ and C_ℓ equal to 100 pF, values which represent a realizable isolation impedance when using a transformer as the output coupler device. For the differential-mode testing, the computer simulation uses the electrode skin impedance model of Chapter Three for gold electrodes of area 2 cm^2. The results for A_d and A_c are shown in Fig. 5.8 and Fig. 5.9 respectively, which also include the effects of battery supply variation.

The results show that the amplifier system fulfills the requirements for measuring electromyographic signals as presented in Chapter Three:

1) a midband gain of 40 db,
2) an upper -3 db frequency point at 1 kHz with a slope of -6 db/octave,
3) a lower -3 db frequency point at 8 Hz with a slope of -12 db/octave.

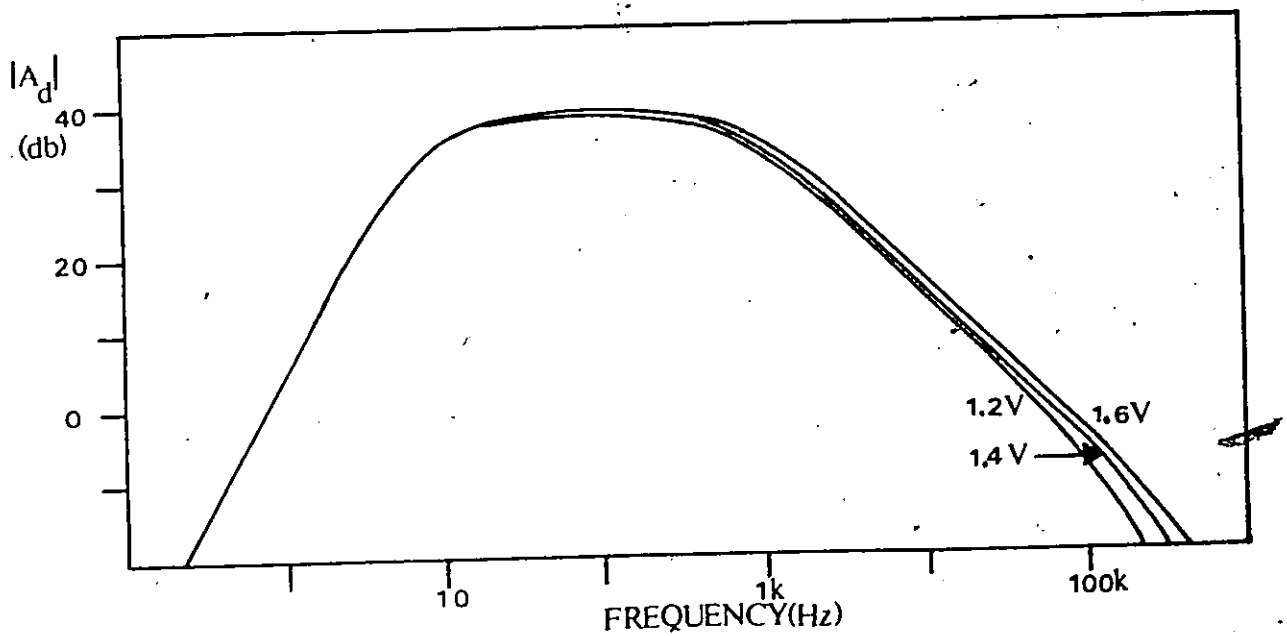

Fig. 5.8 Frequency response of $|A_d|$; computer simulation results for the EMG amplifier design

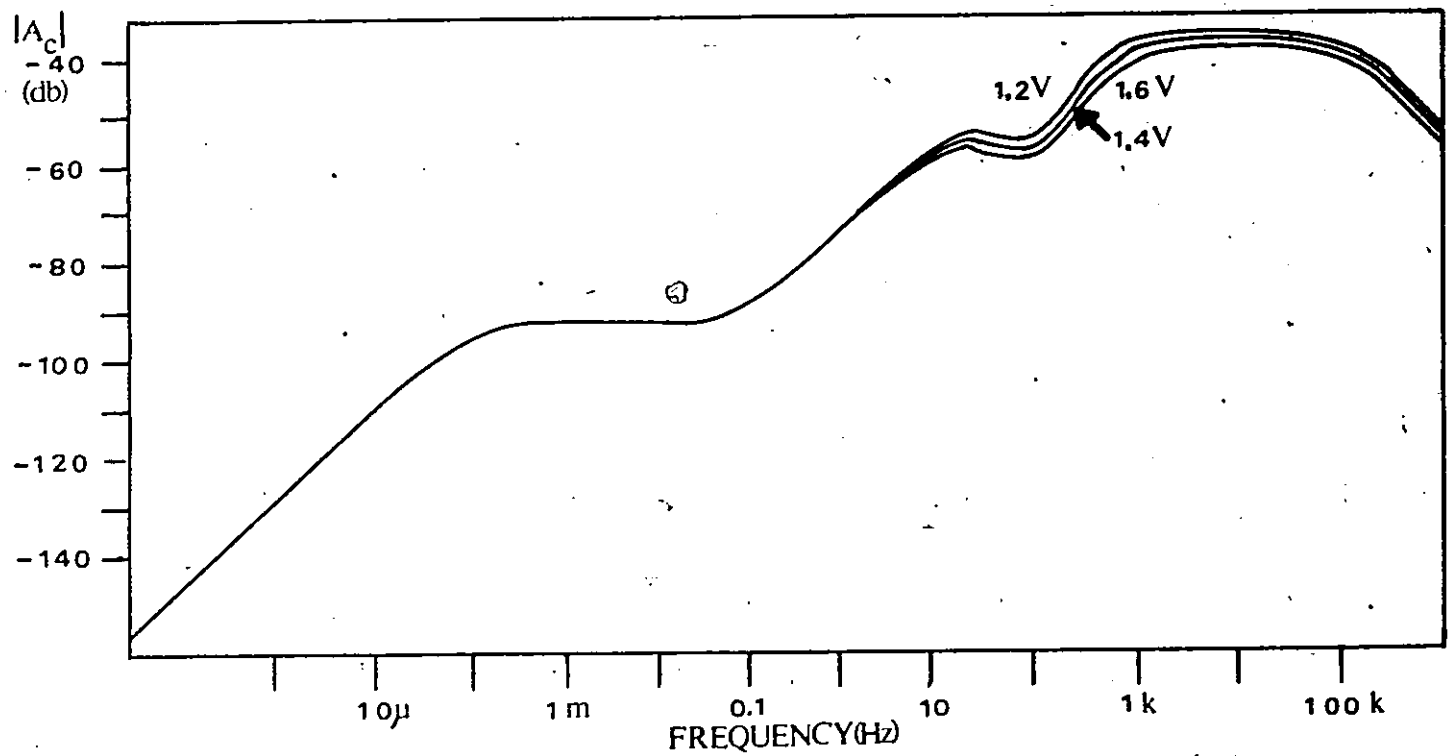

Fig. 5.9 Frequency response of $|A_c|$; computer simulation results for the EMG amplifier design

The common-mode response results are, in comparison to a currently used EMG amplifier system [10], 0.08 times (-25 db) more effective in reducing the most troublesome of common-mode signal source frequencies -60 Hz. The results show that the amplifier system fulfills the common-mode gain requirements for measuring myo-electric signals as presented in Chapter Three where a ground lead is connected to the patient.

It is also seen that battery supply variation does not significantly influence either A_d or A_c.

A transformer was utilized as the output coupler device, which is characterized by isolation properties,

$$C_\ell = 100 \text{ pF} \tag{5.1}$$

$$R_\ell = 10 \text{ G}\Omega \tag{5.2}$$

Electromyograms were taken as shown in Fig. 5.10, using the above described amplifier system with gold electrodes of 2 cm^2, and a low-pass filter on the secondary of the transformer with a -3 db frequency point at 300 Hz with a slope of -6 db/octave. The transformer used did not have the required frequency bandwidth as the lower -3 db frequency point was at 20 hz, but it was judged suitable.

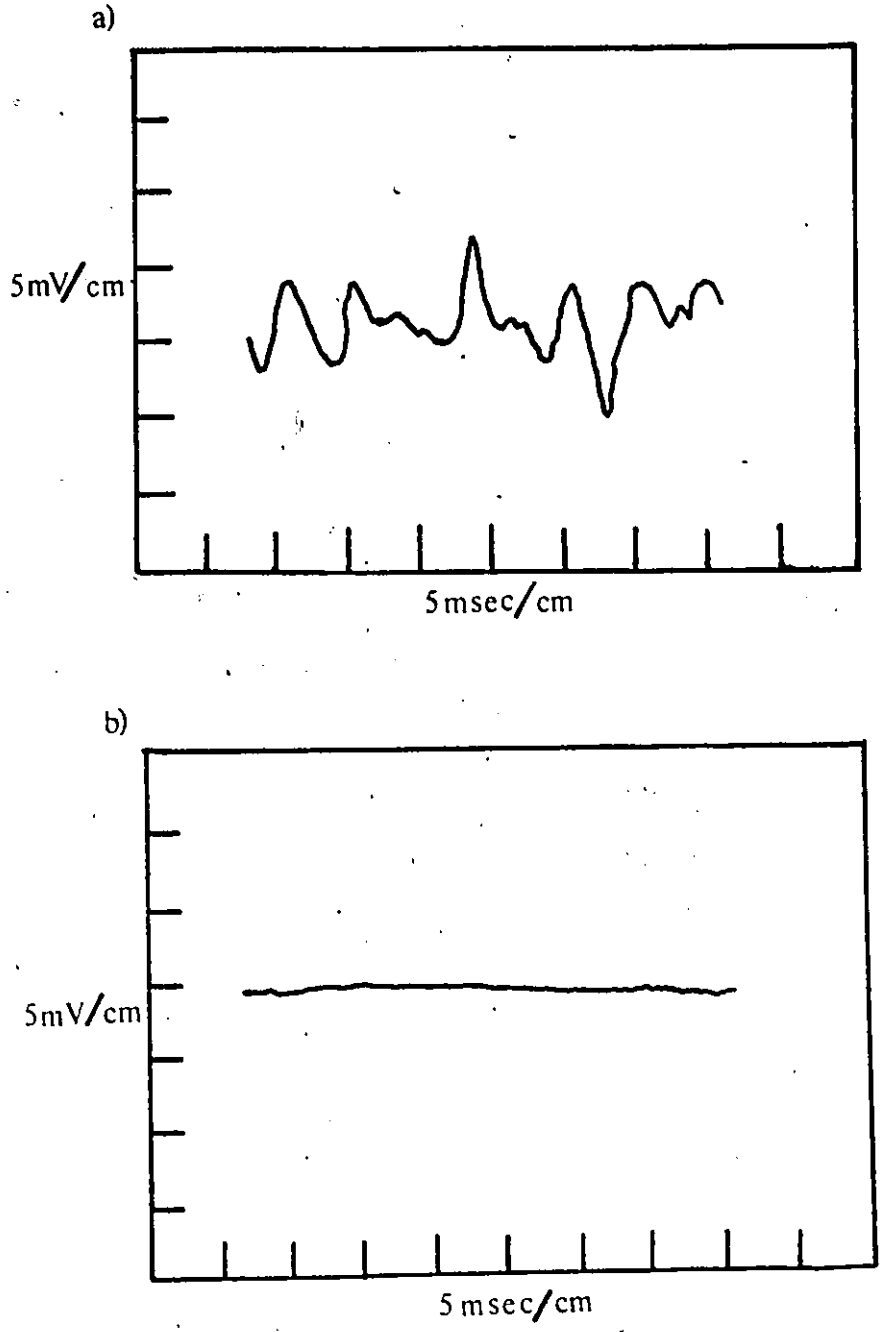

Fig. 5.10 Recorded electromyograms

(a) Muscle contraction

(b) Muscle relaxed

CHAPTER 6

CONCLUSION

In the design of an amplifier wherein the effects of unwanted common-mode signals must be minimized, the benefits of isolating the local ground of the differential amplifier from system ground are not usually recognized. The concept underlying a more general approach which recognizes such benefits, is to break as effectively as possible the common-mode signal path.

In this thesis presentation a more general approach to the problem of unwanted signals arising from common-mode signal sources was developed which includes the non-ideal properties of both the differential amplifier and the output coupler device. It was found that it is possible to write the overall common-mode gain A_c in terms of the product of the differential amplifier common-mode response A_{cv} and the isolation gain A_I. A_{cv} depends on the degree of symmetry of the differential amplifier to reduce the effects of common-mode signals at the differential amplifier input terminals with respect to local ground. A_I depends on the ratio of the isolation impedance to the differential amplifier input impedance.

Whereas A_{CV} may be improved with the use of complex circuits, A_I may be improved by designing the circuit to have a large isolation impedance and a differential amplifier input impedance with limited frequency bandwidth.

In addition, this general approach was shown to reduce the effects of any source impedance mismatch which tends to convert common-mode signals into differential signals.

It was shown possible to model the isolation impedance by a resistor and capacitor in parallel connected between local ground and system ground. Good agreement resulted between experimental data, theory, and computer simulation when this model was used to describe the isolation properties of a transformer. Output coupler devices other than transformers may be used if their energy requirements can be supplied by the self-contained power supply. Examples of output coupler devices which could be used as alternatives are optical, radio-frequency, ultrasonic or acoustical links.

An application of this general approach to the design of an electromyographic amplifier system was illustrated, using a battery as the power supply and a transformer as the output coupler device. The design met the following differential signal frequency response requirements presented in Chapter Three with gold electrodes of area 2

cm^2 and a center-to-center spacing of 2.2 cm:

1) a bandpass amplifier with a midband gain of 40 db,
2) an upper -3 db frequency point at 1 kHz with a slope of -6 db/octave,
3) a lower -3 db frequency point at 8 Hz with a slope of -12 db/octave,
4) a differential input impedance of 1 MΩ shunted by a capacitance equivalent to 0.75 nF.

The isolation properties of the transformer were characterized by an isolation impedance consisting of a resistance/capacitance parallel combination of values 8.8 GΩ/100 pF respectively. When used in conjunction with the differential amplifier, an overall common-mode gain of -55 db at 60 Hz was realized. The final amplifier system design is superior to a currently used design [10], which has only -30 db of common-mode gain at the same frequency. It was demonstrated by theory, computer simulation, and experimental measurement, that for the case where R_ℓ is equal to 10 GΩ, that if C_ℓ is greater than 1 pF, then the limitation on the reduction of A_I and hence A_C is determined by C_ℓ at frequencies in excess of 40 Hz.

In general, it is clear that the isolation capacitance must be minimized to obtain increased common-mode signal rejection by this approach.

APPENDIX A

THE SUBCIRCUIT AMPLIFIER

A.1 Introduction

The subcircuit amplifier shown in Fig. A.1, will be investigated to show that it may be characterized as a single-pole finite-gain voltage amplifier with a fixed input impedance.

This circuit was chosen for the following reasons:

1) an IC chip consisting of all the active components was available,
2) the model parameters for computer simulation of the IC transistors were known,
3) the circuit operates with a single 1.5 volt power supply [13].

For the analysis of the transistors, the modified hybrid-π transistor model [14] was used, as shown in Fig. A.2. It was assumed that the early voltages, V_A, of the NPN and PNP transistors are equal.

The common-mode performance of this circuit was not investigated as Jaeger [1] has shown that this type of circuitry has excellent CMRR properties.

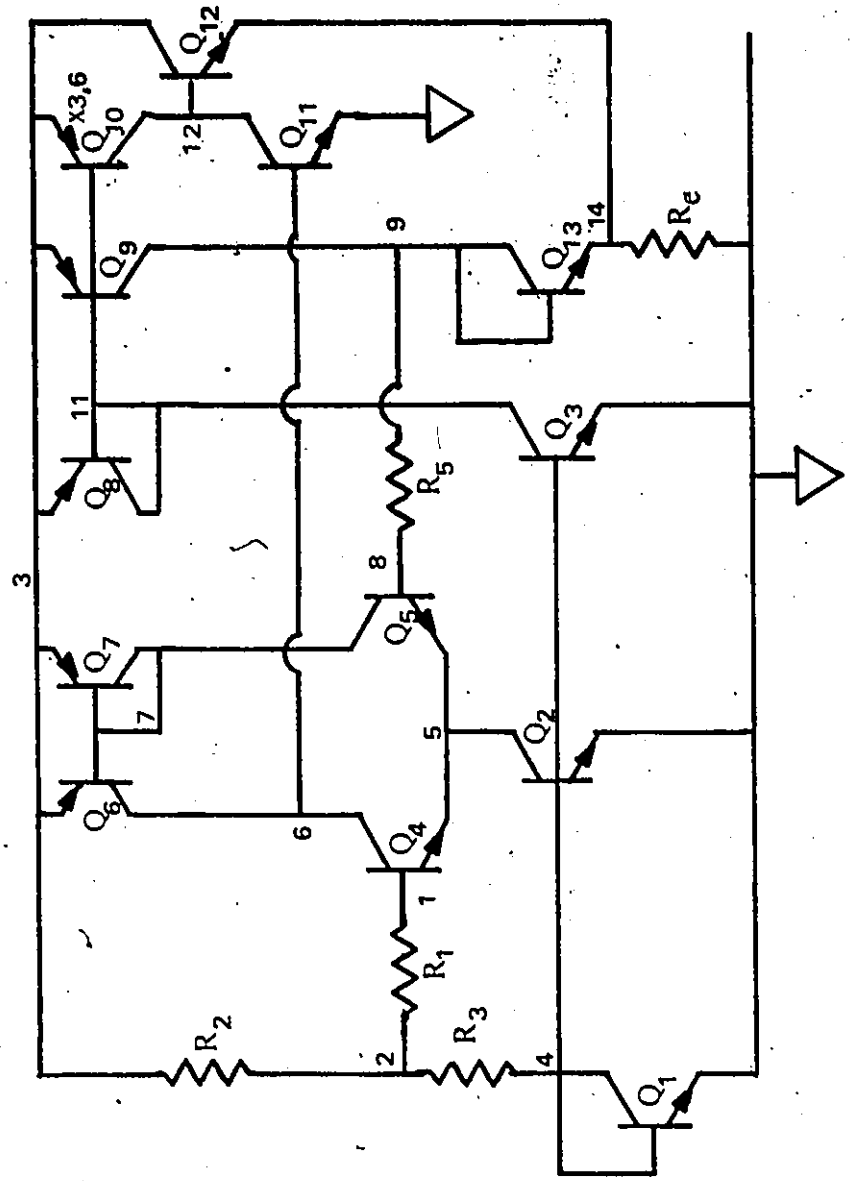

Fig. A.1 The subcircuit amplifier

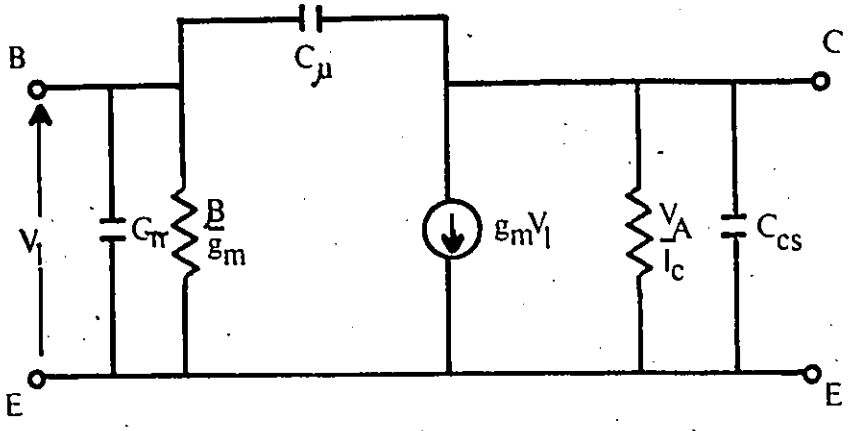

g_m = transconductance = $\frac{I_c}{V_T}$

β = current gain

V_A = early voltage

$V_T = \frac{kT}{q}$

Fig. A.2 Modified hybrid-π transistor model

A.2 Input Impedance

By inspection, the input impedance between the non-inverting input terminal at the base of Q_4 and local ground is

$$R_1 + \frac{R_2 R_3}{R_2 + R_3} \tag{A.1}$$

This assumes that the impedance of Q_4 may be neglected and since Q_1 will be forward biased, it may also be neglected.

As each subcircuit amplifier will be required to have an input impedance equal to approximately 1/2 MΩ, R_1 is chosen to be 470 kΩ.

A.3 The DC Biasing

The dc bias current I_C, always refers to the collector current of Q_1.

Correct dc startup is ensured by the resistor-diode arrangement of R_2, R_3 and Q_1, and by the use of negative dc feedback to the base of Q_5.

The dc bias conditions are found by choosing the dc potential at node 5 to be equal to 0.2 volts. Assuming for simplicity that the base current of Q_4 is zero, then the dc potential at node 2 is

$$.2 + \frac{kT}{q} \ell n \frac{(I_C/2)}{(I_S)} \tag{A.2}$$

R_2 and R_3, establish the collector current of Q_1, and are chosen by

$$R_2 = [1.5 - 0.2 - \frac{kT}{q} \ln (\frac{I_C/2}{I_s})]/I_C \quad (A.3)$$

$$R_3 = [0.2 + \frac{kT}{q} \{\ln (\frac{I_C/2}{I_s}) - \ln (\frac{I_C}{I_s})\}]/I_C \quad (A.4)$$

Two values of bias currents were used.

For

$$I_C = 2.8\ \mu A \quad (A.5)$$

then

$$R_2 = 250\ k\Omega \quad (A.6)$$

$$R_3 = 71\ k\Omega \quad (A.7)$$

For

$$I_C = 10\ \mu A \quad (A.8)$$

then

$$R_2 = 70\ k\Omega \quad (A.9)$$

$$R_3 = 20\ k\Omega \quad (A.10)$$

Due to negative dc feedback, the dc potential at node 14 is equal to 0.2 volts. R_e is chosen to give the desired current in the output stage. R_e was chosen to be equal to 10 kΩ, except for the output amplifier (A_2 of Fig. 4.1) where R_e was set equal to 1.8 kΩ.

A.4 The Low-Frequency Open Loop Voltage Gain [14]

The low frequency open loop voltage gain, A_o, is the product of the gain of three amplification stages:

1) the differential pair Q_4 and Q_5 with the active load pair Q_6 and Q_7,
2) the common emitter stage Q_{11},
3) the emitter follower stage Q_{12}.

The gain of the differential stage is,

$$A_{vdiff} = \frac{V_6}{V_1} = g_{m4} \left(\frac{V_A}{I_{C6}} \,||\, \frac{V_A}{I_{C4}} \,||\, \frac{\beta_{11}}{g_{m11}}\right) \tag{A.11}$$

If

$$\frac{V_A}{I_{C4}}, \frac{V_A}{I_{C6}} >> \frac{\beta_{11}}{g_{m11}} \tag{A.12}$$

and

$$I_{C11} = 3.6\ I_C \tag{A.13}$$

$$I_{C4} = I_{C6} = I_C/2 \tag{A.14}$$

Then

$$A_{vdiff} = \beta_{11}/7.2 \tag{A.15}$$

The gain of the common-emitter stage is

$$A_{v11} = \frac{V_{12}}{V_6} = g_{m11} \left[\frac{V_A}{I_{C11}} \,||\, \frac{V_A}{I_{C10}} \,||\, \left\{\frac{\beta_{12}}{g_{m12}} + R_e(\beta_{12}+1)\right\}\right] \tag{A.16}$$

If

$$\beta_{12} >> 1 \tag{A.17}$$

$$\frac{V_T}{.2} << 1 \tag{A.18}$$

and

$$I_{C11} = I_{C10} = 3.6\ I_C \tag{A.19}$$

$$I_{C12} = .2/R_e \tag{A.20}$$

Then

$$A_{v11} = \frac{3.6\ I_C\ V_A\ R_e\ \beta_{12}}{V_A V_T + V_T I_C R_e (36\beta_{12} V_T + 7.2\beta_{12})} \tag{A.21}$$

The gain of the emitter follower stage is

$$A_{v12} = \frac{V_{14}}{V_{12}} = \frac{1}{1 + \dfrac{\beta_{12}}{g_{m12}(\beta_{12}+1)R_e}} \tag{A.22}$$

and

$$g_{m12} = \frac{.2}{R_e\ V_T} \tag{A.23}$$

then

$$A_{v12} = \frac{.2(\beta_{12}+1)}{.2(\beta_{12}+1)+\beta_{12} V_T} \tag{A.24}$$

Therefore, the low-frequency open loop gain is

$$A_O = \frac{I_C\ V_A\ R_e\ \beta_{11}\ \beta_{12}\ (\beta_{12}+1)}{10[V_A V_T + V_T I_C R_e (36\beta_{12} V_T + 7.2\beta_{12})][.2(\beta_{12}+1)+\beta_{12} V_T]} \tag{A.25}$$

Which may be simplified

$$A_O = \frac{I_C\ V_A\ R_e\ \beta_{11}\ \beta_{12}}{2.26 V_T (V_A + I_C R_e \beta_{12} 7.3)} \tag{A.26}$$

A.5 Frequency Response and Stability

In order to gain insight into the circuit, the frequency response will be determined to a first approximation using a time constant approach [14]. The equivalent circuit of the forward portion of the amplification stages are shown in Fig. A.3 with R_e = 2 kΩ and I_C = 2.8 μA. Table A.I lists the various time constants, which shows that the dominating pole is associated with the base-collector capacitance of Q_{11}. The time constant of the base-collector capacitance of Q_{11}, $t_{\mu 11}$, is

$$t_{\mu 11} = \frac{V_A \beta_{11} \beta_{12} c_{\mu 11} (V_T + I_{C12} R_e)}{2I_{C11} \beta_{12} (V_T + I_{C12} R_e) + V_A I_{C12}} \qquad (A.27)$$

Compensation to the subcircuit amplifier may be achieved by placing capacitors and resistors in parallel with $C_{\mu 11}$. For the IC chips used, internal compensation already exists, 70 pF in series with 5 kΩ in parallel with $C_{\mu 11}$.

To investigate the relative stability of the subcircuit amplifier with compensation, Bode plots of the open loop gain were obtained using computer simulation. When a 1 F capacitor is placed between nodes 8 and 10, dc feedback is maintained but the ac feedback is removed so that the subcircuit amplifier operates at its open loop gain.

The phase at unity gain must be less than 135° to

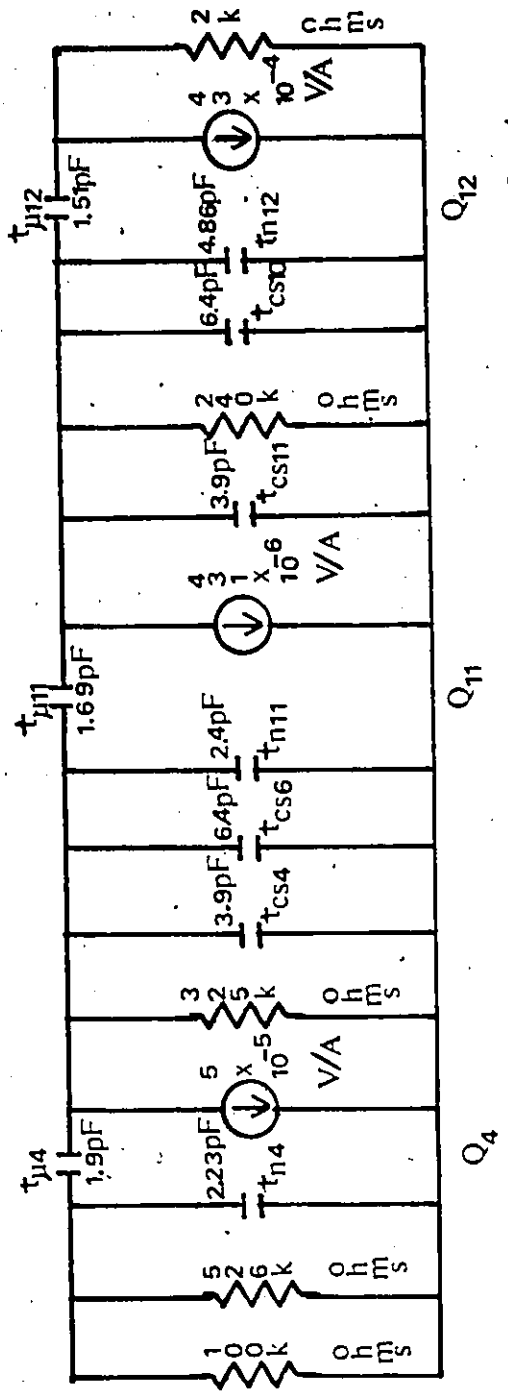

Fig. A.3 The equivalent circuit model for the time constant analysis

Table A.I Time Constants

t	EVALUATION	μ sec
$t_{\pi 4}$	84 kΩ x 2.23 pF	0.187
$t_{\mu 4}$	5×10^{-5} A/V x 84 kΩ x 325 kΩ x 1.9 pF	2.6
t_{cs4}	3.9 pF x 325 kΩ	1.27
t_{cs6}	6.4 pF x 325 kΩ	2.08
$t_{\pi 11}$	2.41 pF x 325 kΩ	0.78
$t_{\mu 11}$	1.69 pF x 431 x 10^{-6} A/V x 325 kΩ x 240 kΩ	56.8
t_{cs11}	3.9 pF x 240 kΩ	0.936
t_{cs10}	6.4 pF x 240 kΩ	1.54
$t_{\pi 12}$	4.86 pF x 240 kΩ	1.17
$t_{\mu 12}$	1.51 pF x 4.3 x 10^{-3} A/V x 2 kΩ x 240 kΩ	3.116

ensure an adequate stability margin [15]. Figures A.4, A.5, A.6, A.7 show that adequate stability margin exists for all combinations of I_C = 2.8 μA, 10 μA and R_e = 1.8 kΩ, 10 kΩ. Due to this stability margin, any circuit which uses the subcircuit amplifier in any of the four possible configurations should be stable.

A.6 Subcircuit Amplifier Model

The subcircuit amplifier input impedance between the non-inverting terminal at the base of Q_4 and local ground is equal to 500 kΩ, and similarly the feedback resistance between the inverting terminal at the base of Q_5 to the output node 14 is equal to 500 kΩ. Table A.II presents the open loop gain and the -3 db frequency point obtained both by theory (A.25 and A.27) and by computer simulation. Figures A.4 - A.7, all show a characteristic single pole response. Therefore the subcircuit amplifier may be modelled as a single-pole finite-gain voltage amplifier as,

$$V_0 = \frac{A_O\ (V_1 - V_8)}{(1 - s/p_A)} \qquad (A.28)$$

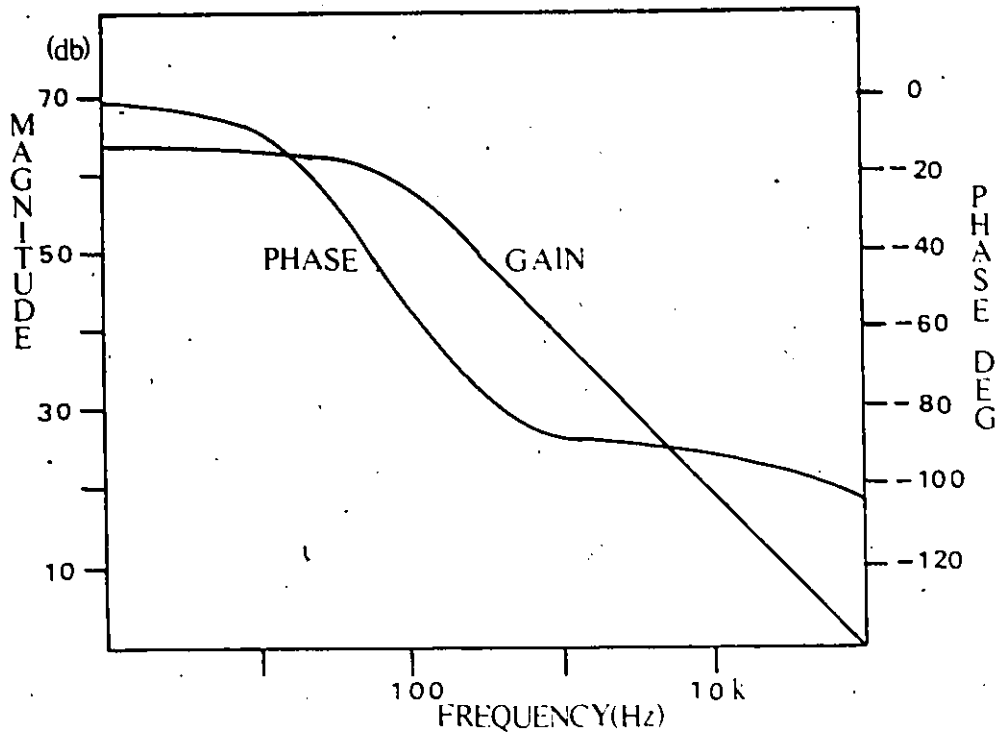

Fig. A.4 Bode plot of the subcircuit amplifier open loop gain, I_C= 2.8 μA, R_o= 1.8 kΩ

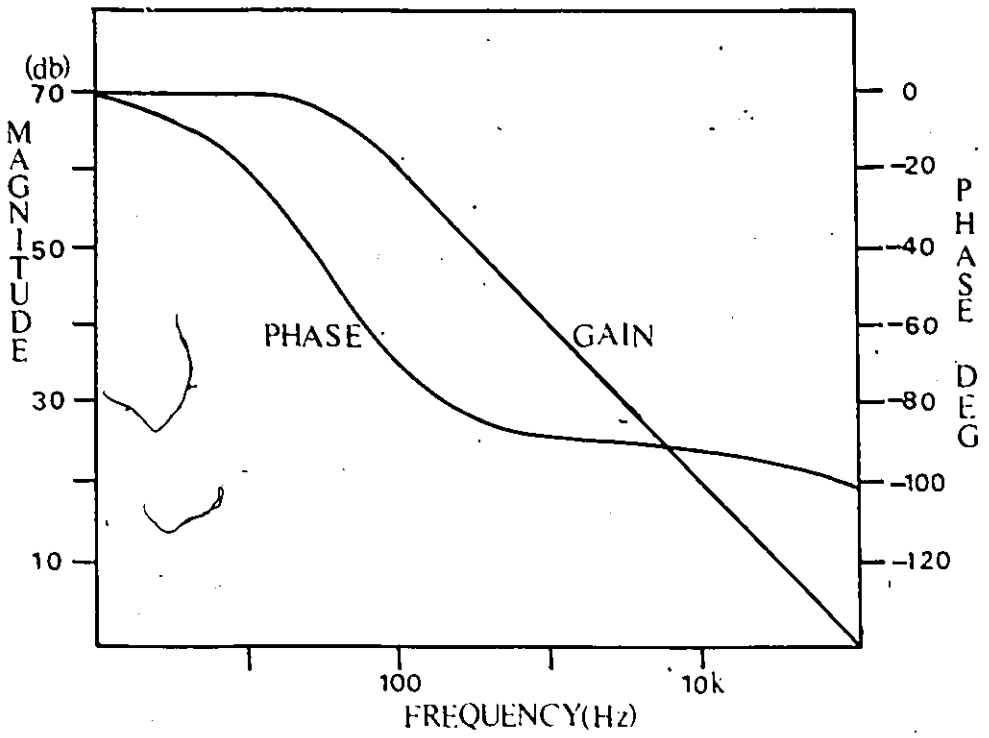

Fig. A.5 Bode plot of the subcircuit amplifier open loop gain, I_C= 2.8 μA, R_e= 10 kΩ

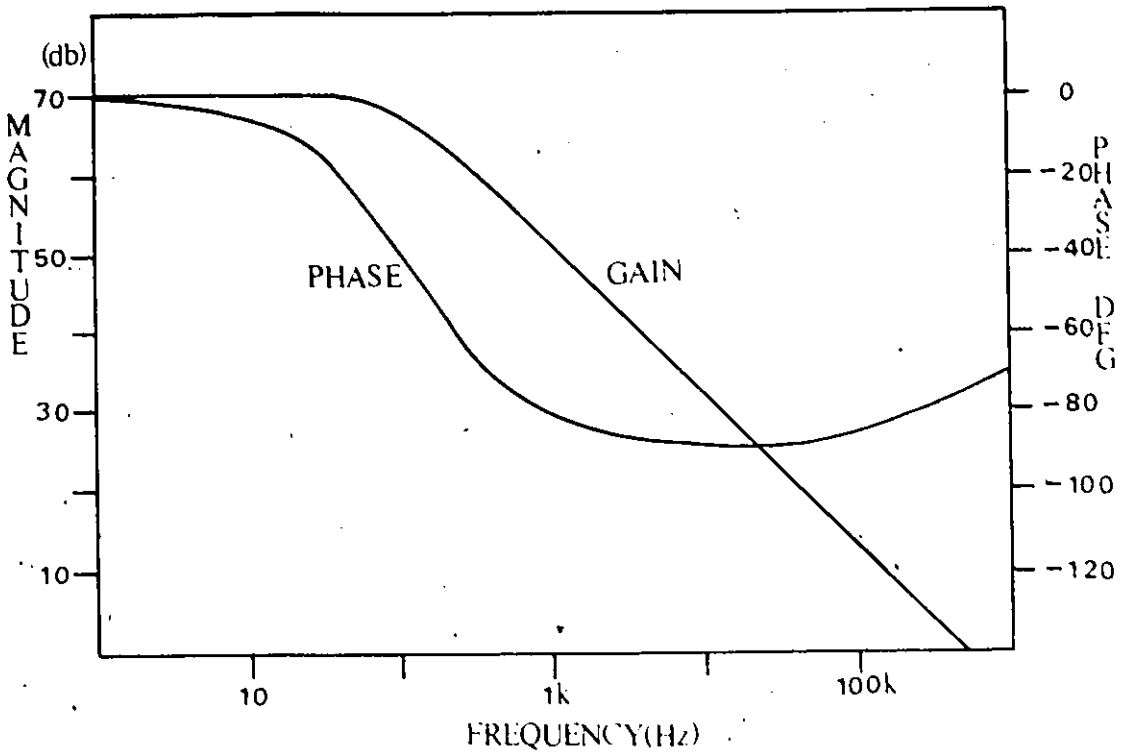

Fig. A.6 Bode plot of the subcircuit amplifier open loop gain, I_C= 10 μA, R_e= 1.8 kΩ

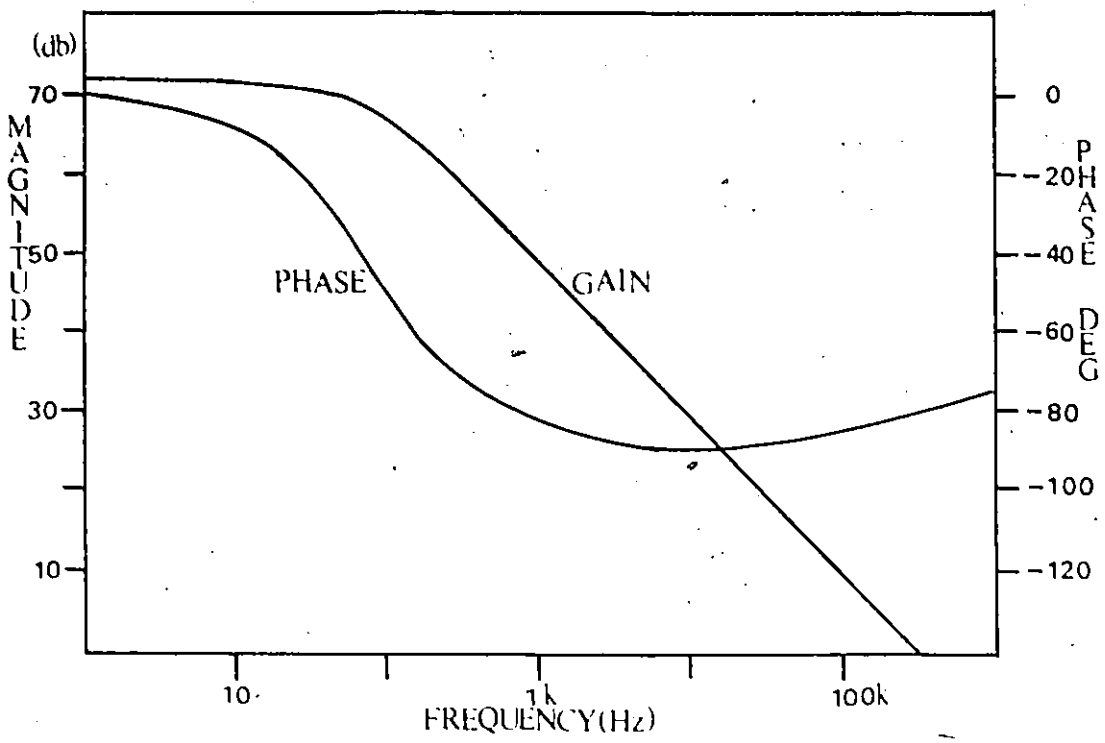

Fig. A.7 Bode plot of the subcircuit amplifier open loop gain, I_C= 10 μA, R_e= 10 kΩ

Table A.II Subcircuit Amplifier Parameters

		A_o		p_A	
I_C	R_e	THEORY	SPICE	THEORY	SPICE
2.8 μA	1.8 kΩ	63.8 db	63.7 db	57 Hz	63 Hz
	10 kΩ	69.8 db	70 db	31 Hz	31.6 Hz
10 μA	1.8 kΩ	69.9 db	70 db	105 Hz	112 Hz
	10 kΩ	71.8 db	71.7 db	80 Hz	89 Hz

REFERENCES

[1] R.C. Jaeger, "Common Mode Rejection Limitations of Differential Amplifiers", IEEE Journal of Solid-State Circuits, SC-11, no. 3, p. 411, June 1976.

[2] J.C. Graeme, Application of Operational Amplifiers Third-Generation Techniques, Toronto, McGraw-Hill, 1973.

[3] L.W. Nagel, SPICE2, A Computer Program to Semi-Conductors Circuits, University of California at Berkely, Memorandum ERL M520, 9 May, 1975.

[4] Dorland, Dorland's Illustrated Medical Dictionary, 25th Edition, Philadephia, Saunders, 1974.

[5] L.A. Geddes and L.E. Baker, Principles of Applied BioMedical Instrumentation, New York, Wiley, 1968.

[6] Private Communication, Technical Staff, Dept. of BioMedical Engineering, Chedoke Hospital, Hamilton, Canada.

[7] G.E. Bergey, R.D. Squires, and W.C. Sipple, "Electrocardiogram Recording with Pasteless Electrodes", IEEE Trans. on BioMedical Eng., BME-18, no. 3, p. 206, May 1971.

[8] L.A. Geddes, C.P. Da Costa, and G. Wise, "The Impedance of Stainless Steel Electrodes", Med. & Bio. Engng., vol. 9, p. 551, 1971.

[9] M.S. Spach, et. al., "Skin-Electrode Impedance and its Effect of Recording Cardiac Potentials", Circulation, vol. 34, p. 649, Oct. 1966.

[10] J.V. Basmajian and J.E. Hudson, "Miniature Source Attached Differential Amplifier for Electromyography", American Journal of Physical Medicine, vol. 53, no. 5, p. 234, 1974.

[11] Private Communication, Dr. H. de Bruin, Chedoke Hospital, Hamilton, Canada.

[12] H.W. Tam and J.G. Webster, "Minimizing Electrode Motion Artifact by Skin Abrasion", IEEE Trans. on BioMedical Eng., BME-24, no. 2, p. 134, March 1977.

[13] Private Communication, Dr. D.H. Barber, Linear Technology Inc., Burlington, Canada.

[14] P.R. Gray and R.G. Meyer, Analysis and Design of Analog Intergrated Circuits, Toronto, Wiley, 1977.

[15] J.G. Graeme, G.E. Toby, and L.P. Huelsman, Operational Amplifiers: Design and Applications, Toronto, McGraw-Hill, 1971.